CHAPTER - IV

LINEAR AROMATIC POLYESTERS AS EFFECTIVE CORROSION MITIGATORS FOR MILD STEEL IN 0.5 M H_2SO_4

4.1 INTRODUCTION

Mild steel owing to its high mechanical strength and low cost has established itself as one of the leading and prominent material in construction, pipelines, refineries, chemical and electrochemical industries[1]. It is preferred to be a choice of raw material due to its interesting properties such as hardness, ductility, lustre, malleability and good conductivity. Unfortunately these properties get deteriorated when such metals interact with certain elements within the environmental proximity or when subjected to industrial practices like acid pickling, acid cleaning and descaling, undergoes a process technically referred as corrosion.

Pertaining to the environmental impacts and global issues, significant progress has been made in various aspects to synthesise corrosion inhibitors to minimise the rate of metal dissolution and acid consumption. However it is noteworthy that the compounds used as corrosion reducers must full fill the following basic requirements[2]

- Should get oxidised to form impervious film
- Capable of adsorbing on the metal surface
- Should cover large surface and eco-friendly
- it should be readily available and safe in handling

Based on the above criteria, lot of researchers have worked to synthesise inhibitors under the cluster of organic and inorganic compounds. The less yielding nature of inorganic inhibitors has limited its usage.

Generally organic compounds with heteroatoms like N, O or S carrying lone pair of electrons, aromatic ring and pi-conjugated system undoubtedly behaves as efficient corrosion inhibitors[3-11] protecting the metal specimens either by undergoing physical[12] or chemical adsorption[13]. But its tedious synthetic methodology and exorbitant prices has led to severe criticisms paving way towards polymeric compounds. Besides enormous reports filed towards organic corrosion inhibitors, attention towards polymers in minimising metal dissolution is

increasing nowadays due to extensive delocalization of p electrons which makes it to behave as better inhibitors than organic compounds[14]. As an attempt of finding perfect replacement for the existing inhibitors, a long term research has begun gearing towards polymeric materials whose availability, cost effectiveness, eco friendliness in addition to its inherent stability and multiple adsorption centres has made it as specific choice of interest.

Considering all these factors, the present chapter has been undertaken to study the anticorrosive nature of linear aromatic cardo polyesters (shown in chapter II) as a perfect replacement for existing organic and inorganic inhibitors. To strengthen our discussion, a glimpse of previous work reported has been reviewed and presented below.

4.1.1 Review of literature

Hitoshi Okuda *et al.,* designed 9,9-(4-hydroxyphenyl)- 4,5-diazafluorene (N-BPF) as a novel cardo structure followed by examining the properties of poly(ether ketone)s (N-PEKs) incorporated with N-BPF. The resulting N-PEKs were credited with cardo characteristics such as high thermal stability and high solubility. This was further added with p-toluenesulfonic acid (TsOH) to exhibit polymeric network of good refractive index, flexibility and transparency[15].

An attempt to synthesise aromatic polyesters containing bulky flourene cardo moieties from 9,9-bis(4-carboxyphenyl)fluorine was made by **Guey-Sheng Liou *et al.,*.** The cardo based synthesis resulted with the polymers of good thermal stability, high glass transition temperature, photolumniscent, optically transparent and electrochromic in nature[16].

Hyeonuk Yeo *et al.,* utilised bis-thienyl-benzothiadiazole as a co monomer to introduce mono and di substituted cardo flourenes combined with boron dipyrromethene (BODIPY) into conjucated polymer. Good solubility, film forming ability, strong dual emission property, colour tunability were observed in the resulting polymers[17].

Wang *et al.,* reported the synthesis of cardo polyimides involving both fluorinated and non-fluorinated diamines with aromatic anhydrides. Compared to aromatic polyimides, the synthesised cardo polyimides possessed better thermal property and high glass transition temperature. Observation of fluorinated and non-fluorinated polymers revealed that the fluorinated polymers were of better solubility, hydrophobicity, high optical transparency and low dielectric constant[18].

Xuhai Xiong *et al.,* designed bismaleimide oligomers containing novel aryl-ether-imide/cardo phthalide in different molecular weights followed by its structural elucidation

using Fourier transform infrared (FTIR) spectroscopy and nuclear magnetic resonance (^{1}H and ^{13}C NMR) spectroscopy. Amorphous nature was revealed from XRD measurements. Thermal analysis was made by DSC and TGA analysis. It was further concluded that the phthalide cardo structure introduced brought enhanced properties of the synthesised polymers[19].

Agnieszka Iwan *et al.,* successfully synthesised novel polyazomethine on the basis of thiophene and cardo groups where the resulting polymer was characterised using FTIR and ^{1}H NMR spectroscopy followed by its application in solar cells[20].

Grafting of poly(ethylene oxide) (PEO) with cardo poly(aryl ether sulfone) (PES-NH) was performed by **Shuhua Hou *et al.,*** to synthesise amphiliphilic copolymers (PES-g-PEO). The involvement of cardo moieties imparted hydrophilicity, high thermal and mechanical stability which promised the resulting graft co polymer in fabricating antifouling membrane[21].

Nian Gao *et al.,* adopted nucleophilic substitution reactions to synthesise cardo poly(arylene ether sulfone)s using 3,3-bis(4-hydroxyphenyl)-1-isobenzopyrrolidone and 4,4-difluorodiphenylsulfone or 3,3,4,4-tetrafluorodiphenylsulfone and sulfoalkyl agents. The resulting polymer was characterised by FT-IR and ^{1}H NMR spectroscopy and the membranes obtained were used as polyelectrolytes for proton exchange fuel cells[22].

Bisphenol monomer with electron rich tetraphenylmethane substituents were utilised by **Jifu Zheng *et al.,*** to synthesise sulfonated cardo poly(arylene ether sulfone)s (SPES-x). The polymeric membrane resulted with good thermal, mechanical and film forming ability with lower methanol intrusion. Values observed were more than nafion membrane, hence more promising in methanol fuel cells[23].

Roy *et al.,* in 1998 synthesised cardo polyphosphonates which were thermally stable by means of interfacial polycondensation. The structural studies were made based on IR, ^{1}H and ^{31}P NMR spectroscopy. Thermal analysis carried out showed the weight loss at 350^{o}C. The polymers resulted with good amorphous nature and good solubility in polar aprotic solvents as well as chlorinated aliphatic hydrocarbons[24].

Hohyoun Jang *et al.,* utilised hydrophilic and hydrophobic oligomers to synthesise sulphonated multiblock poly(arylene ether sulphone) copolymers (SMPESs) comprising of phenolphthalein anilide cardo group. FT-IR, ^{1}H-NMR and TGA studies were carried out for the synthesised copolymers[25].

Vibhute *et al.,* utilised phenolphthalein and *m*- and *p*-toluidines as precursors to synthesise phthalides containing bisphenols, phenolphthalein-*N*-(3-methylanilide) (3-PMA), and phenolphthalein-*N*-(4-methylanilide) (4-PMA). Interfacial or solution polymerisation techniques were adopted for synthesis. 93–99% yield of polymers with reduced viscosity, ready solubility, excellent glass transition temperature and stability was observed. A discussion on structure-property relationship of cardo polyesters were also made[26].

Fomenkov *et al.,* studied the molecular mass of cardo poly(benzimidazoles) using GPC analysis. Depending on the reaction conditions like temperature, time and concentration of the reactants, formation of microgels was studied allowing the reaction between 4,4'-oxydibenzene-1,2-diamine and 4,4'-(3-oxo-1,3-dihydroisobenzofuran-1,1-diyl)dibenzoic acid in the presence of Eaton's reagent[27].

Haixiang Sun *et al.,* utilised solution polymerisation technique to synthesise cardo polyimide/TiO_2 mixed matrix membrane. The synthesised membrane was characterised by FTIR, ^{1}H NMR, DSC and XRD analysis. Various tests carried out towards gas separation techniques made it as a promising candidate for the same[28].

Pushan Wen *et al.,* synthesised two novel cardo polyimides by the polymerisation of 2,7-diamino-9,9-spirobifluorene (2,7-DASBF) with 4,4'-(hexafluoro isopropylidene) diphthalic anhydride and pyromellitic dianhydride. Structural elucidation followed by thermal analysis were carried out for the synthesised polymers[29].

Blanco *et al.,* adopted solvent free reaction to prepare sulfonated polymer namely sulfonated polyethersulfone cardo at various degrees by controlling the time and temperature. Longer reaction time and higher temperature lead to the higher sulfonation resulting in hydrophilic polyelectrolytes making it suitable for ultra and nano filtration[30].

Desai *et al.,* targeted cardo polysulfonates originating from 1′-bis (4-hydroxy phenyl) cyclohexane with benzene-1,3-toluene-2,4-disulfonyl chlorides in 1:1 ratio in presence of cetyl trimethyl ammonium bromide, an emulsifier. The structure of the polymers synthesised were characterised using IR and NMR spectral analysis followed by evaluating its biological activity[31].

Based on the above literature, it can be generally agreed that the footprint of polymers in various applications is remarkable. However the quench towards various needs has tuned the researchers to move towards the high performance polymers (HPPs) in early 1960's. On

scrutinising, polyimides, poly(amideimide)s, aromatic polyesters and polyamides are considered as significant HPPs where the present discussion is about to go with the aromatic polyesters. In general HPPs, are accompanied with high rigidity, crystallinity and melting point, low solubility and strong intermolecular interactions which makes its processing tedious. To overcome these limitations, any of the following methods can be adopted as stated and illustrated below.

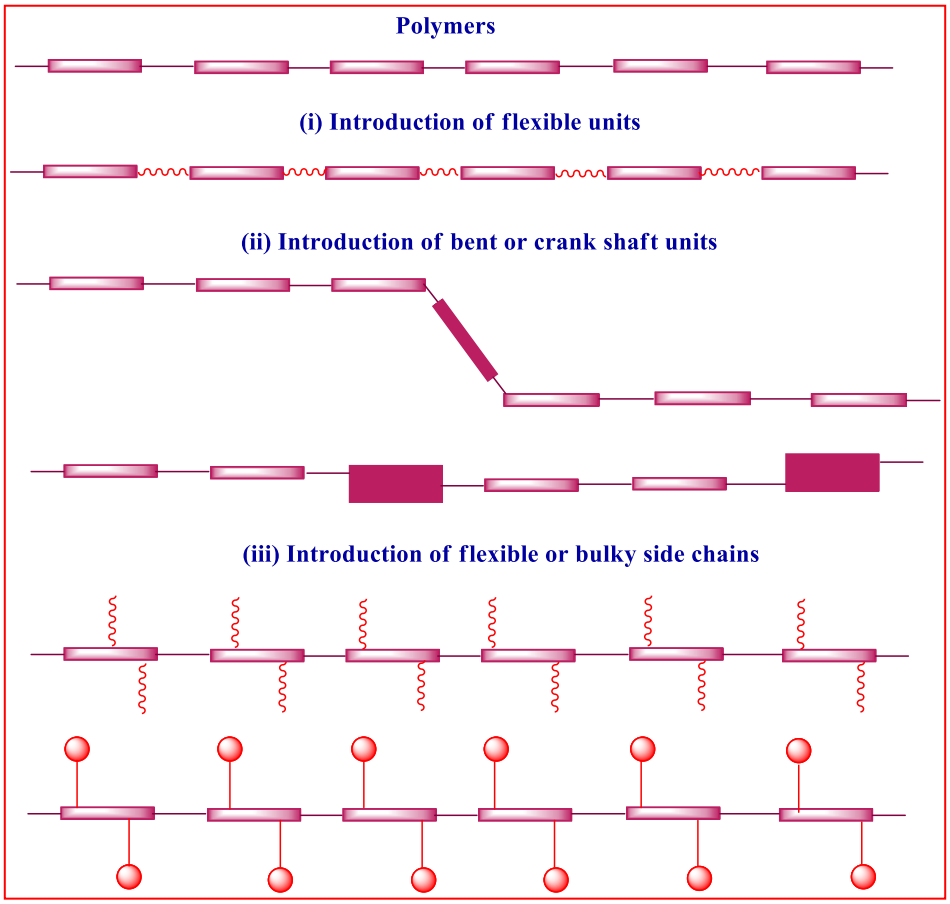

(i) Inserting flexible spacers between rigid structure

(ii) Inserting a bent or crankshaft to make random or alternate copolymers.

(iii) Appending bulky or flexible moieties within the aromatic backbone.

Polyesters, a class containing –COO groups in main chain was first enlightened by Conix in 1957 through a reaction between dicarboxylic acid and diphenols which has deserved considerable interest due to its mechanical, thermal and chemical stability[32]. But polyesters with high aromatic content makes its processing difficult because of insolubility in organic solvents and high T_g values[33-35]. As a destination to improve the polymeric properties, the above mentioned modification can be brought into the monomers. Introducing cardo groups

which is referred as “hinge” or “loop” in Latin, has the capability of increasing the solubility and decreasing T_g values without affecting the thermal stability[36,37] because of its reduced intermolecular interactions followed by higher internal mobility of polymeric chains. Such specificity of cardo moieties has intended us to synthesise a series of polyesters containing cardo groups and to evaluate its anticorrosive potential towards mild steel in aggressive acid medium which has not been reported elsewhere.

4.2 EXPERIMENTAL METHODS

4.2.1 Inhibitors

A series of cardo polyesters synthesised using dicarboxylic acids and its corresponding acid chlorides as outlined below (discussed in detail in chapter II) were subjected as inhibitors for mild steel in acid medium in the present investigation.

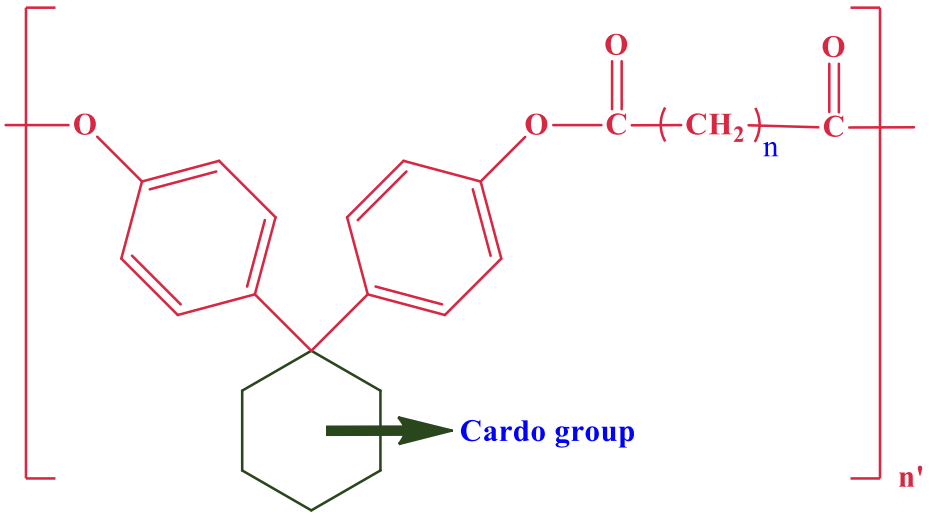

Where **n=1**, 4-(1-(4-methoxyphenyl)cyclohexyl)phenyl 3-oxobutanoate **(MPOB)**

n=2, 4-(1-(4-methoxyphenyl)cyclohexyl)phenyl 4-oxopentanoate **(MPOP)**

n=3, 4-(1-(4-methoxyphenyl)cyclohexyl)phenyl 5-oxohexanoate **(MPOHX)**

n=4, 4-(1-(4-methoxyphenyl)cyclohexyl)phenyl 6-oxoheptanoate **(MPOHP)**

n=5, 4-(1-(4-methoxyphenyl)cyclohexyl)phenyl 7-oxooctanoate **(MPOO)**

n=6, 4-(1-(4-methoxyphenyl)cyclohexyl)phenyl 8-oxononanoate **(MPON)**

n=7, 4-(1-(4-methoxyphenyl)cyclohexyl)phenyl 9-oxodecanoate **(MPOD)**

n=8, 4-(1-(4-methoxyphenyl)cyclohexyl)phenyl 10-oxoundecanoate **(MPOU)**

4.2.2 Material preparation

The mild steel working specimens containing major proportion of iron were selected and made into appropriate dimensions as required for electrochemical and non-electrochemical techniques. The corrodent 0.5 M H_2SO_4 was prepared from the analar grade sulphuric acid using distilled water. The metal specimens were abraded with various grades of emery sheets until a mirror finish was ensured.

4.2.3 Evaluation of anticorrosive performance

(a) Gravimetric measurements

Gravimetric method is the simplest method to estimate the corrosion rate in which the experiments were conducted under total immersion period of three hours using 100 ml beakers containing various concentrations of the polymers (10, 50, 100, 500, 1000 ppm) in 0.5 M H_2SO_4. The precleaned and weighed specimens were suspended in triplicates with the aid of glass hooks in order to ensure the reliability of the results. The specimens were retrieved after 3 hours, washed, dried and reweighed. Using semi micro analytical balance the loss in mass was calculated and the mean values were computed to determine the necessary parameters. The efficiency of the selected concentration of the inhibitors were evaluated at high temperature in the range 313 K-333 K in a thermostatic water bath for an immersion period of 1 hour. Various parameters such as inhibition efficiency (I.E)[38], surface coverage (Θ), corrosion rate (CR) and thermodynamic parameters were derived from the following relationship

Inhibition efficiency (I.E)	
$I.E\ (\%) = \frac{CR_o - CR_{inh}}{CR_o} X100$	(1)
Corrosion rate (CR)	
$CR\ (gcm^{-2}hr^{-1}) = \frac{534\ X\ weight\ loss(gms)}{Density\ X\ Area\ (cm^2)\ X\ Time\ (hrs)}$	(2)
Surface coverage (Θ)	
$\Theta = \frac{CR_o - CR_{inh}}{CR_o}$	(3)
Activation energy (E_a)	

$$E_a = 2.303 \text{ X } 8.314 \text{ X slope} \quad (4)$$

Free energy of adsorption (ΔG^o)

$$\Delta G^o{}_{ads} = -RT\ln(55.5K) \quad (5)$$

(b) Electrochemical measurements

To study the kinetics of the corrosion inhibition process as well as cathodic and anodic partial reactions occurring, a three electrode set up was assembled with a mild steel working electrode of 0.785 cm^2 exposed area, a platinum and calomel electrode as counter and reference electrodes. Prior to each run, the working electrode was polished to mirror finish and placed in 0.5 M H_2SO_4 test solution and the necessary electrochemical data were computed from the installed IVIUM software.

(i) Electrochemical impedance spectroscopy (EIS)

EIS measurements were performed at measured OCP in the frequency range of 10 KHz to 0.01 Hz with an amplitude of 10 mV peak to peak. From the resulting Nyquist complex plane representation (Z' Vs Z''), the charge transfer resistance (R_{ct}) and the double layer capacitance (C_{dl}) were calculated and the inhibition efficiencies were determined using the following equation.

$$\text{Inhibition efficiency (\%)} = \frac{R_{ct(inh)} - R_{ct(blank)}}{R_{ct(inh)}} X100 \quad (6)$$

where charge transfer resistance in inhibited and uninhibited medium is represented as $R_{ct(inh)}$ and $R_{ct(blank)}$.

(ii) Potentiodynamic polarisation method

This technique was carried out from cathodic potential of -200 mV to anodic potential of +200 mV at scan rate of 1mV/sec. From the intercept of extrapolated Tafel lines, corrosion current density (i_{corr}) was determined. From the following relation the inhibition efficiencies were evaluated,

$$\text{Inhibition efficiency (\%)} = \frac{I_{corr(blank)} - I_{corr(inh)}}{I_{corr(blank)}} X100 \quad (7)$$

where $I_{corr(blank)}$ & $I_{corr(inh)}$ represents corrosion current in the absence and presence of inhibitor.

4.2.4 Morphological examination

(i) FT-IR spectra of metal specimens

To evaluate the possibility of various sites involved in adsorption, the surface film formed on the mild steel specimen after immersing in 1000 ppm of MPOB and MPOU were evaluated using ATR-FT-IR spectrometer (Shimadzu).

(ii) X-ray diffraction analysis

The mild steel specimens of appropriate dimensions were immersed in 0.5 M H_2SO_4 test medium and the corrodent with 1000 ppm of inhibitors MPOB and MPOU for 3 hours after which they were retrieved, washed, dried and subjected to X-ray diffraction measurements in the angle range of $10^o < 2\Theta < 80^o$.

(iii) Scanning electron microscopy (SEM) and Energy dispersive X-ray spectroscopy (EDS)

As an additional evidence, the surface layer formed on the metal specimens after polishing and immersing in optimum concentration of polymer was examined using Zeiss electron SEM microscopic analyser incorporated with energy dispersive X-ray spectroscopy to detect the elemental composition.

(iv) Atomic force microscopy (AFM)

Inspection of the surface film formed on the mild steel surface was still dealt in detail by subjecting the metal specimens to AFM analysis using multimode scanning probe microscope (NT-MDT) followed by the results projected in the form of roughness values.

(v) X-ray photoelectron spectroscopy (XPS)

Surface morphological examination was carried out for the metal specimens immersed in electrolyte containing 0 ppm and 1000 ppm concentration of the inhibitor, MPOU using Model no-Axis ultracompany – Kratos Analytical country-UK XPS spectrometer, employing a source of Al K alpha (1486 eV). Experimental photopeaks were simulated and quantified by casaxps software.

4.3 RESULTS AND DISCUSSION

4.3.1 Gravimetric method

The effect of inhibitors on the mild steel owing to a decreased corrosion rate with increased concentrations (10, 50, 100, 500, 1000, 1500 ppm) are summarised in the **Table 4.1**. It is obvious from the data and **Fig. 4.1**, that all the polymers inhibit the dissolution of mild steel relying with concentration (up to 1000 ppm) added in 0.5 M H_2SO_4 medium. Beyond 1000 ppm, further increase in concentration of inhibitors up to 1500 ppm resulted with decreased inhibition efficiency based on which 1000 ppm was optimised. It is generally agreed that the primary action of inhibition process is by adsorption of polymer on metal surface which in turn gives an idea about the extent of surface covered (Θ) by the polymer[39]. This inhibitive action can be explained on the basis of the lone pair electrons on the oxygen atom which contributes to the adsorption through donor-acceptor bond between the non-bonding electron pairs and the vacant orbitals of the metal surface[40]. The increase in number of methylene units favours + inductive effect rendering greater extent of surface coverage which is evident from the highest inhibition efficiency of 92.98% at 1000 ppm exhibited by MPOU. Moreover its surface coverage 0.9298 approaching unity indicates almost full coverage of the surface[39] by the added polymer. In addition, the presence of aromatic moieties in the present series favours increased inhibition efficiency compared to the aliphatic ones (chapter iii) due to its aromatic anchoring sites.

(a) Effect of temperature

The action of aromatic polyesters at high temperature (303 K-333 K) was evaluated by performing weight loss experiment for selected concentration of the inhibitors for a duration of 1 hour. From the **Table 4.2**, it is clear that inhibition efficiency decreases with increase in temperature which might be attributed due to the shorter time gap between the adsorption and desorption of the polyesters over the metallic surface staying exposed to the acidic environment for a longer time[41] leading to increased corrosion rate. As reported by **Anusuya *et al.,***[1], increased enthalpy values impairs some of the chemical bonds responsible for adhering on the surface thereby reducing its stability and shifting the inhibitor-metal interfacial equilibrium leading to desorption of molecules.

(b) Kinetic considerations

Relation between corrosion rate of mild steel and temperature of the environment is expressed by the following Arrhenius equation

$$\text{Corrosion rate (CR)} = A\exp^{[(-Ea)\,/\,RT]} \tag{8}$$

Transition State equation, a modified form of Arrhenius equation lead to the calculation of enthalpy and entropy of activation based on the following relationship

$$\text{Corrosion rate (CR)} = RT/Nh \exp(\Delta S^o / R) \exp(-\Delta H^o / RT) \quad (9)$$

where E_a is the energy of activation, ΔS^o and ΔH^o represents enthalpy and entropy of activation, A is the Arrhenius pre exponential factor, h is the Planck's constant, N is Avogadro number, T is the absolute temperature and R represents universal gas constant.

Kinetic Representation	**Verification plot**	**Slope**	**Intercept**
Arrhenius equation	log CR Vs 1000/T	$-E_a / RT$	-
Transition equation	log CR/T Vs 1/T	$-\Delta H^o$ /2.303R	$\log(R/Nh) + (\Delta S^o /$ 2.303R)

Detailed illustration of the Arrhenius and Transition State plots displayed in the **Fig. 4.2** and **Fig. 4.3** predicts various parameters as listed in **Table 4.3**. It is clearly revealed from the table that increase in energy of activation from 51.81 KJ/mol (uninhibited) to 72.52 KJ/mol (MPOP inhibited) can be attributed to an appreciable decrease in the adsorption of polymers on the mild steel surface with increase in temperature representing physical adsorption[42]. The E_a values in presence of polymers were observed to be higher than those of uninhibited 0.5 M H_2SO_4 solution suggesting the increased energy barrier on addition of inhibitors. Higher values of E_a lowers the corrosion rate or corrosion current density indicating that the electron transfer in oxidation-reduction process becomes less dense thereby retarding the corrosion rate[43]. The endothermic nature pertaining to tough dissolution of mild steel is revealed from the positive values of ΔH^o. From **Table 4.3,** it can be observed that variation of E_a and ΔH^o seems to be similar where $E_a > \Delta H^o$ represented simple hydrogen evolution reaction[44]. The –ve values of ΔS^o represents association rather than dissociation meaning that decrease in disorderness takes place on going from reactants to activated complex owing to more ordered behaviour leading to increased inhibition efficiency.

Further to gain insight into the adsorption mechanism, heat of adsorption (Q) can be evaluated from the kinetic – thermodynamic expression as represented below,

$$\log\frac{\theta}{1-\theta} = \log A + \log C - \left[\frac{Q_{ads}}{2.303RT}\right] \quad (10)$$

where A is a constant, C is the inhibitor concentration, Θ is the occupied sites, 1-Θ represents the vacant sites.

Fig. 4.4 depicts a plot of log (Θ/1- Θ) as a function of 1000/T for the various concentrations of the inhibitor. From the slope of the linear plots the values of heat of adsorption (Q) were estimated which is equal to (– Q/2.303*R) and listed in **Table 4.3**. Negative values of Q_{ads} obtained indicates decreased inhibition efficiency with increase in temperature supporting the proposed physisorption mechanism[44].

(c) Adsorption isotherm

Adsorption is one of the critical factor that decides the performance of an inhibitor on the metal surface. Study of adsorption isotherm helps us to understand the kind of interaction between inhibitor and metal surface. It is usually a quasi-substitution process where the replacement of adsorbed water molecules by the inhibitor occurs. The nature of adsorption of polymers on mild steel in 0.5 M H_2SO_4 solution was assessed by fitting the calculated surface coverage (Θ) values into various adsorption isotherms namely Langmuir, Temkin, El-Awady and Flory Huggins isotherms. Basically all the tested isotherms are generally represented as[45],

$$f(\Theta.x)\exp(-2a\Theta) = K_{ads}C$$

where f(Θ.x) is the configuration factor depending on the physical model and assumptions , 'a' is the molecular interaction parameter, Θ is the surface coverage, K_{ads} is the equilibrium constant and C represents the concentration.

The Karl Pearson's co-efficient (correlation co-efficient) obtained from fitting the experimental results are displayed in **Table 4.4**. It is revealed from the data that $R^2 > 0.9$ and good linear relationship proved the best fit with Langmuir adsorption isotherm supporting the monolayer adsorption which has a general representation,

$$\frac{C}{\theta} = \frac{1}{K_{ads}} + C$$

where C, Θ, K_{ads} is the concentration, surface coverage and adsorption co-efficient.

Based on the R^2 values and the adsorption plots shown in **Fig. 4.5(a-d)**, strong deviation of Temkin, El-Awady and Flory-Huggins isotherms were observed. The best fit was observed with Langmuir adsorption isotherm. The relationship between K_{ads} and ΔG^o involving the universal gas constant (R) and absolute temperature (T) as shown are listed in the **Table 4.4**.

$$\Delta G^o = -RT\ln K_{ads}$$

The ΔG^o parameter evaluated from the best fitted Langmuir adsorption isotherm acquired negative charge implying spontaneous adsorption of inhibitors on the mild steel surface[46] and the magnitude was found to be below -40 kJ/mol. On scrutinising the literature, most of the researchers have reported that the ΔG^o up to -20 kJ/mol represents physisorption whereas ΔG^o more than -40 kJ/mol endeavours chemisorption[47]. As reported by **Chaitra *et al.*,**[41] none of the inhibitor can get adsorbed on the metal surface purely by physical or chemical adsorption. Negative values of ΔG^o confirmed the spontaneous adsorption favouring complex comprehensive interaction, incorporating both physical and chemical adsorption due to the increased oxygen atoms and pi-electrons leading to the film formation favouring decreased metal dissolution[43].

(d) Thermodynamic considerations

Thermodynamic model enables us to understand the adsorption phenomena of inhibitor molecules. The enthalpy of adsorption (ΔH^o) calculated from the Vant Hoff equation as represented below is listed in **Table 4.5**,

$$\ln K_{ads} = -\Delta H^o_{ads} / RT + \Delta S^o_{ads} / T + \ln 1/55.5$$

Similarly Gibbs Helmholtz relationship shown below enables to calculate the enthalpy of adsorption (ΔH^o).

$$\Delta G^o_{ads} / T = \Delta H^o_{ads} / T + A$$

Figs. 4.6 and 4.7 predicts the plot of log K_{ads} Vs 1/T and $\Delta G^o_{ads}/T$ Vs 1/T which results in straight lines with a slope and intercept equal to $\Delta H^o_{ads}/2.303R$ and $\Delta S^o_{ads}/2.303R$ +1/55.5 in the former and a slope directly related to ΔH^o_{ads} in the latter case. Plot of ΔG^o_{ads} vs T as shown in **Fig. 4.8** was also in good agreement with the results evaluated.

It is generally observed that the endothermic adsorption process ($\Delta H^o_{ads}>0$) is attributed unequivocally to chemisorption whereas ($\Delta H^o_{ads}<0$) represents exothermic adsorption process

involving physisorption or chemisorption or both[44] which correlates well with the present ΔH^{o}_{ads} values. However the values of ΔG^{o} obtained in the range of -29.88 kJ/mol to -34.77 kJ/ mol favours predominantly physisorption and a slight chemisorption[48]. As per the above mentioned statement, the ΔH^{o}_{ads} derived from van't Hoff and Gibbs Helmholtz equation predominantly supports physisorption mechanism.

4.3.2 Electrochemical measurements

(a) Electrochemical impedance spectroscopy (EIS)

The EIS technique allows the evaluation of the kinetics of electrochemical processes and the inhibition mode occurring at the mild steel and 0.5 M H_2SO_4 interface modified by the presence of selected concentrations of the polymers. The impedance values were measured at open circuit potential (OCP) and were analysed by fitting into Randle's equivalent circuit as shown in **Fig. 1**

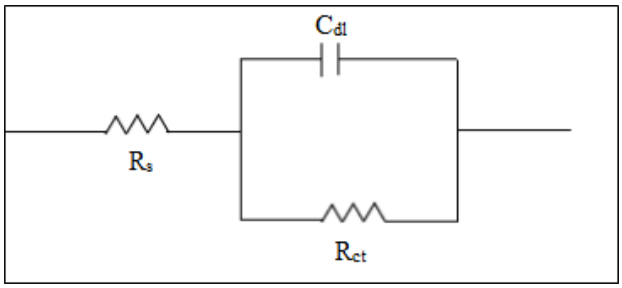

Fig. 1 Randles equivalent circuit

where solution resistance, charge transfer resistance and double layer capacitance are indicated by R_s, R_{ct} and C_{dl} .

(i) Nyquist plot

The impedance data measured for mild steel in 0.5 M H_2SO_4 is displayed in the form of Nyquist plot (Z' vs Z''). Nyquist plots predicted in **Figs. 4.9 - 4.16**, shows single capacitive semicircles indicating that the charge transfer process is controlling the corrosion and the depressed loops might be due to the frequency dispersion and micro roughness of the electrode surface[49]. From the data represented in the **Table 4.6**, it is evident that the R_{ct} values increases from 15.8 ohm cm^2 (blank) by the successive addition of inhibitors indicating the strengthening of the film[50]. A large charge transfer resistance indicates that the system is corroding more slowly where the inhibitor molecules adsorb onto the surface of the metal forming a barrier. The double layer between the electrolyte and metal surface is considered as electrical capacitor.

The inhibitor molecules remove water molecules and other ions that were adsorbed on the metal surface, thus reducing its electrical capacity. The inhibitor molecules must have a lower dielectric constant to be able to displace the water molecules which have a higher dielectric constant. The inhibitive action on the mild steel surface increases by adsorption of the added inhibitor on the steel surface leading to the reduction of the active surface area exposed to the aggressive medium[51] which is evident from the plots by the increased diameter of the semicircles.

On investigating the polymers at any selected concentration, MPOU exhibits better inhibition efficiency which might be attributed due to the increased alkyl spacers and benzene rings in its structure which is supposed to increase the electron cloud on the molecules in turn increasing the adsorption ability[47] compared with the rest of polymers which possess lesser number of alkyl moieties. With an increase in surface coverage, thickness of the adsorbed layer increased by replacing the pre adsorbed water molecules and other ions gradually resulting in lowered C_{dl} values[52]. Nyquist plots are more informative to investigate the dominant corrosion mechanism either kinetically controlled (semicircle) or diffusion controlled (straight line). The semicircle shape of the plots represent kinetic controlled corrosion dominating diffusion controlled mechanism[53] which is exhibited by a large capacitive loop at high frequency followed by a small inductive loop at low frequency. The capacitive loop is attributed to the charge transfer controlled corrosion phenomena, whereas the inductive loop corresponds to the relaxation process obtained during the adsorption of inhibitor on the electrode surface[54].

(ii) Bode plot

Bode plot affords more reliable information compared to Nyquist plot. It is a method of evaluating the EIS data which shows the effect of angular frequency on the impedance and the phase angle shift (Θ). It is generally observed that smaller the value of Θ_{max} higher will be the surface roughness. Plots displayed in **Figs. 4.17 – 4.24** shows Θ_{max} of -23^o for blank which gets successively increased on addition of inhibitors implying the reduced surface roughness thereby retarding corrosion rate. Since frequency appears as one of the axes, it is easy to understand the dependence of impedance on frequency. The bode format seems to be desirable since it provides clear description of electrochemical systems frequency dependent behaviour than Nyquist plot in which small frequency values are implicit. These plots exhibit linear portions at intermediate frequencies. The linearity of log |Z| vs log f at intermediate frequency

are more pronounced in presence of inhibitors than the blank suggesting the pseudo-capacitive behaviour at the electrode surface[55].

These plots are useful since they can define a domain of pure capacitive behaviour and can be divided in to three sectors as,

i. At high frequencies, the phase angle decreases to almost zero and this is characteristic of a response to resistive behaviour.

ii. At intermediate frequencies, the maximum phase angles are obtained at various concentrations of inhibitor indicating interference capacitance.

iii. At low frequencies, the phase angle becomes near to zero which is a response of inductive behaviour[42].

Ideally, the phase angle should be -90° which is indicative of capacitive behaviour[41]**.** The difference between the maximum phase angle and -90° is thought to be due to deviations that arise from ideal capacitive behaviour. Thus in the presence of inhibitors, the phase angle gradually approaches the nearest ideal capacitive value thereby slowing down the dissolution rate of metal attaining a steady state.

(b) Potentiodynamic polarisation technique

The corrosion behaviour of metals and alloys can be evaluated using potentiodynamic polarization curves. This method is also known as potential sweep, cyclic voltammetry or linear sweep voltammetry. This technique widely used in electrochemistry measures the current that develops from varying the electrode potential between a selected range. The polarisation curves of mild steel in 0.5 M H_2SO_4 for the selected concentrations of the inhibitor are shown in **Figs. 4.25-4.32** and the data are listed in **Table 4.7**. It is evident from the values that there is a prominent decrease in the corrosion current densities pertaining to the adsorption of inhibitors on the active sites of the metallic surface, thereby retarding the metal dissolution (I) and the hydrogen evolution (II) as shown resulting in slowing down the corrosion process

$$Fe_{(S)} \longrightarrow Fe^{2+}{}_{aq} + 2e^- \qquad (I)$$

$$2H^+ + 2e^- \longrightarrow H_{2(g)} \qquad (II)$$

Under the experimental conditions performed, the cathodic branch (potentials negative of OCP, i.e., corrosion potential, E_{corr}) represents current related to the hydrogen evolution

reaction occurring on the MS surface, while the anodic branch (potentials positive of OCP) represents the actual corrosion reaction, i.e., iron dissolution. The cathodic and anodic current branches display linear regions, confirming that the two partial reactions (hydrogen evolution and metal dissolution) are under kinetic control[56] .These two linear parts represented so-called Tafel slopes, and they intersect at OCP yielding the total corrosion current (I_{corr}). The decrease in I_{corr} values indicates the response of the inhibitor towards mild steel incorporated with increased inhibition efficiency. The observed E_{corr}, b_a and b_c values does not show predominant change after the addition of polymers neither interfering with the anodic dissolution nor cathodic H_2 evolution independently but performs in a mixed nature[53]. The present result confirms the adsorption by the π electrons of aromatic ring co-existing with lone pair of electrons of oxygen atoms. The mixed type is further supported by the displacement of E_{corr} values < 85 mV[41] which is 23.7 mV in the present evaluation. Generally polymeric molecules can inhibit either by occupying reactive sites or simply providing resistance to the supply of oxidant or transporting the reaction products away from the metal surface[39]. The results obtained from the electrochemical and non-electrochemical methods are in good agreement with the same magnitude[57] but the slight variation observed may be due to the period of immersion or the occlusion of the metal surface from inhibitor formulation.

4.3.3 Morphological examination

(i) FT-IR spectra of metal specimens

As an insight of finding the possibility of functional groups involved in adsorption, FT-IR spectra was recorded for the protective layer formed on the metal surface[44]. Analysis of spectra of inhibited plates shown in **Fig. 4.33**, revealed >C=O shift from 1733.83 cm^{-1} and 1719.61 cm^{-1} to 1700.78 $cm^{-1}$and 1738.90 cm^{-1} in MPOB and MPOU inhibited specimens followed by >C-O-C< shift of MPOB from 1227.05 cm^{-1} to 1206.13 cm^{-1} and 1224.85 cm^{-1} to 1249.81 cm^{-1} for MPOU inhibited compared to MPOB and MPOU. Also a prominent shift observed for $–CH_2$ units from 2926.34 cm^{-1} and 2919.39 cm^{-1} to 2974.43 cm^{-1} and 2988.62 cm^{-1} (inhibited) in case of both polyesters, indicated the possibility of methylene units favouring adsorption on the metal surface. The >C=C< stretching of aromatic ring shifted from 1518.22 cm^{-1} to 1531.77 cm^{-1} for MPOU and in case of MPOB from 1630.07 cm^{-1} to 1524.81 cm^{-1} showing the involvement of aromatic pi-electrons[49]. All these shifts observed concluded the involvement in adsorption enhancing the bond formation.

(ii) X-ray diffraction pattern

The main phases observed in a corroded specimen are lepidocrocite (g-FeOOH), goethite (a-FeOOH) and magnetite (Fe_3O_4). Lepidocrocite is formed at early stages of atmospheric corrosion whose time exposure transforms it into goethite. The X-ray diffraction patterns observed for uninhibited specimens revealed intense peaks at $2\Theta = 37.62^o$, 43.92^o and 81.98^o corresponding to various iron oxide corrosion products[58]. Examining the XRD patterns displayed in **Fig. 4.34,** the enhanced peak intensity due to corrosion products were successively reduced in presence of inhibitors suggesting the protective layer formation on the mild steel surface. Moreover the peaks observed approximately at $2\Theta = 80^o$ due to iron[59], the major proportion of the preferred specimens get suppressed on addition of MPOB and MPOU suggesting that the added inhibitors has covered the surface of the metal thereby retarding its dissolution.

(iii) Scanning electron microscopy (SEM) and Energy dispersive X-ray spectroscopy (EDS)

Observation of the SEM micrographs shown in **Fig. 4.35(a)**, depicted rough surface (blank) with cavities insisting that the mild steel specimen has undergone severe corrosive attack. On the other hand, close observation of **Fig. 4.35(b-c)** inhibited with MPOB and MPOU exhibited smoother surface which would have been formed by the added polymers on gradual filling of cavities resulting in the formation of barrier on the metal surface thereby minimising the exposure of metal specimen to the aggressive medium[60] which imparts reduced metal dissolution.

The EDS spectra of corroded specimen shown in **Fig. 4.35(a)**, exhibited the characteristic sharp peaks of iron and oxygen indicating the enhanced corrosion process resulting in the formation of iron oxide product when metal specimen is immersed in uninhibited medium. The EDS recorded for the specimens immersed in 0.5 M H_2SO_4 containing 1000 ppm of MPOB and MPOU displayed in **Fig. 4.35(b,c)**, projected lower intensity of iron peaks along with carbon and oxygen signals which revealed that the surface is covered by the added inhibitors resulting in enhanced inhibition thereby suppressing the dissolution of mild steel[52] which correlated well with the elemental composition represented in **Table 4.8**.

(iv) Atomic force microscopy (AFM)

AFM is an emerging morphological analysis technique from nano to micro scale based on root mean square values (S_q), average roughness (S_a) and peak to valley (P-V) height. The high values of S_q, S_a and P-V height of uninhibited medium recorded as 312.40 nm, 244.27 nm, 2855.15 nm implied rough, corrosive, bumpy structure as shown in **Fig. 4.36(a)**. On comparing the appearance and roughness data (S_q, S_a and P-V height) of inhibited specimens with uninhibited ones, lower values of inhibited specimens observed as 243.71 nm, 217.26 nm, 2355.98 nm for MPOB and 172.37 nm, 139.18 nm, 1741 nm for MPOU suggested the possibility of forming Fe^{2+} - polymer complexes owing to a relative smoother surface of MPOU compared to MPOB which can be visualised from the AFM images displayed in **Fig. 4.36(b,c)**.

(v) X-ray photoelectron spectroscopy (XPS)

In order to investigate the composition of the adsorbed species on the metal specimen, XPS analysis was carried out and displayed in **Fig. 4.37**. The spectra C 1s, Fe 2p and O 1s shown exhibited complex forms assigned to its own corresponding species obtained from deconvolution fitting procedure. Observation of Fe 2p spectra (**Fig. 4.37**) of uninhibited specimen showed a peak at 711.8 eV owing to the presence of ferric compound. Fe 2p spectra of MPOU inhibited specimen, showed two peaks at 711.8 eV and 714.2 eV corresponding to the iron compounds like Fe_2O_3 and FeOOH which is stable and insoluble forming a protective layer on the metal surface thereby reducing the diffusion of ions towards the aggressive medium[61]. Peak at 725.6 eV (higher binding energy) represented Fe(II) species which could enable the formation of MPOU-Fe(II) complex on the metal surface thereby protecting the specimen. O 1s spectra recorded for blank showed peaks at 529.6 eV and 532.8 eV corresponding to O^{2-} and OH^- followed by the O 1s deconvoluted spectra of MPOU with two peaks at 532.4 eV and 533.9 eV which would be due to OH^- of FeOOH and –C=O bond present in additive. C 1s deconvoluted spectra predicted in **Fig. 4.37** is associated with two different peaks both for blank and MPOU inhibited specimen. However based on broadness of the peak observed for inhibited specimen, one could assume the involvement of carbon attached to various groups in film formation on the metal surface. Thus the first peak at 285.1 eV could be attributed to –C-C-, -C=C-, -C-H aromatic bonds and other hydrocarbons whereas the second peak at 289.1 eV corresponded to –C-O linkage as predicted under O 1s. Based on the above discussion, XPS analysis favours the formation of film on the metal surface which is quite complex in nature, insoluble and stable.

4.3.4 Mechanism of adsorption

Generally it is observed that the Fe_2O_3 layer formed on the metal surface in the atmosphere acts as a partial barrier until the metal is subjected to pickling[56] in acid medium as follows,

$$Fe + Atmosphere \longrightarrow Fe_2O_3$$

Out of the various processes, pickling forms the basic step which is incorporated with the following reactions with the evolution of hydrogen

$$M + H_3O^- + e^- \longrightarrow H_2O + MH_{ads}$$

$$MH_{ads} + MH_{ads+} \longrightarrow 2M + H_2$$

In order to minimise the evolution of hydrogen, polymers were added successively to protect the metals from some detrimental effects[44]. The added polymers gets protonated in acidic medium where the metal protection was afforded by the presence of oxygen atoms, $>CH_2$ units and aromatic sites favouring the unshared electron pairs of nucleophilic atoms and pi-electron density of aromatic ring as adsorption sites on the metal surface. The protonated polymer interacts on the metal-solution interface by adopting any of the following ways.

i) Electrostatic interaction of protonated polymer with already adsorbed SO_4^{2-}ions

ii) Interaction between pi-electrons of aromatic ring and vacant d-orbital of iron

iii) Interaction between lone pair of electrons and vacant d-orbital of iron

On the other hand, an electrostatic repulsion arises between the metal bearing positive charge and protonated polymer hindering the way to minimise the metal dissolution. But the lower degree of hydration of SO_4^{2-}ions brings excess negative charge at the vicinity favouring interaction with protonated polymers leading to the complex formation as evident from surface morphological studies. Initially the mild steel dissolution in acidic medium involves the formation of FeOH and $[FeSO_4OH]^{2-}$ as intermediates which were later converted into stable complexes after the intervention of polymers as reported by **Sangeetha *et al.*,**[49]. **Fig. 4.38** predicts the schematic illustration of the above suggested mechanism.

$$Fe^{2+} + xH_2O + YSO_4^{2-} + Polymer(Inh) \longrightarrow [Fe(Inh)(OH)_x(SO_4)_y]^{2-x-y} + xH^+$$

4.3.5 Evaluation of inhibitors

The corrosion inhibition studies of the synthesised polymers were incorporated with decreased corrosion rate with increased concentration. These polymers inhibited the metal dissolution by getting adsorbed at the Fe-electrolyte interface. Among the investigated polymers MPOU exhibited the highest inhibition efficiency whereas MPOB showed the least inhibitory action and the intermediate polymers brought the successive increase. This was primarily attributed due to the increased $–CH_2$ units which in turn increased bulkiness favouring

good attachment at adsorption sites thereby retarding the corrosion rate[42]. In general all the inhibitors primarily gets adsorbed on to the metal surface either through its functional groups or through the presence of nucleophilic atoms such as N, O, S, P (or) multiple bonds (or) aromatic sites present in the molecular structure. All the polymers applied in the present investigation contains oxygen as nucleophilic attachment site with similar structure but differed only in the length of aliphatic moieties ($-CH_2$ units). Thus the length of the aliphatic units behave as a deciding factor in bringing inhibition efficiency which is additionally pronounced with the aromatic units[39] in the present synthesised polymers as good anchoring sites whose absence shows lesser inhibition efficiency comparatively as discussed in chapter III. Based on the above discussion, the present set of polyesters can be arranged in the following order according to their inhibition efficiency.

MPOU > MPOD > MPON > MPOO > MPOHP > MPOHX > MPOP > MPOB

Observations made prove that the increase in the number of carbon atoms increases the surface coverage thereby retarding the contact between metal-solution interface resulting in decreased corrosion rate and increased inhibition efficiency which is evident from the highest inhibition efficiency of 92.98% for MPOU and lowest for MPOB around 79.88%.

4.4 CONCLUSIONS

The following conclusions can be revealed from the above discussion.

(i) Results of weight loss measurements revealed decreased corrosion rate with increased concentration rendering higher inhibition efficiency of 92.98% for MPOU and minimum of 79.88% for MPOB.

(ii) Increasing temperature from 303 K – 333 K showed decreased inhibition efficiency.

(iii) Free energy of adsorption parameter emphasised predominantly physisorption.

(iv) Experimental data for the investigated cardo polyesters seemed to be best fitted with Langmuir adsorption isotherm favouring monolayer adsorption.

(v) Increased charge transfer resistance observed from impedance measurements suggested the formation of a barrier on the metal surface.

(vi) Polarisation measurements exhibited retardation of both cathodic and anodic partial reactions with predominantly cathodic effect.

(vii) Surface morphological studies done by FT-IR, XRD, SEM, EDS, AFM and XPS supported the surface coverage by the added inhibitors.

(viii) Out of the various methods adopted in the present discussion, all the techniques favoured inhibition efficiency in the following trend

MPOU > MPOD > MPON > MPOO > MPOHP > MPOHX > MPOP > MPOB

4.5 REFERENCES

1. N. Anusuya, J. Saranya, P. Sounthari, A. Zarrouk, S. Chitra, J. Mol. Liq., **225** (2017) 406-417.
2. T. Douadi, H. Hamani, D. Daoud, M. Al-Noaimi, S. Chafaa, J. Taiwan. Inst. Chem. E., **71** (2017) 388-404.
3. H. Zarrok, H. Oudda, A.E. Midaoui, A. Zarrouk, B. Hammouti, M.E. Touhami, A. Attayibat, S. Radi, R. Touzani, Res. Chem. Intermed., **38** (2012) 2051-2063.
4. P. Mourya, P. Singh, R.B. Rastogi, M.M. Singh, Appl. Surf. Sci., **380** (2016) 141-150.
5. M. Bouanis, M. Tourabi, A. Nyassi, A. Zarrouk, C. Jama, F. Bentiss, Appl. Surf. Sci., **389** (2016) 952-966.
6. X. Ma, X. Jiang, S. Xia, M. Shan, X. Li, L. Yu, Q. Tang, Appl. Surf. Sci., **371** (2016) 248-257.
7. M. Gopiraman, N. Selvakumaran, D. Kesavan, R. Karvembu, Prog. Org. Coat., **73** (2012) 104-111.
8. H. Zarrok, A. Zarrok, R. Salghi, M.E. Touhami, H. Oudda, B. Hammouti, R. Touir, F. Bentiss, S.S. Al –Deyab, Int. J. Electrochem.Sci., **8** (2013) 6014-6032.
9. E.B. Ituen, O. Akaranta, S.A. Umoren, J. Mol. Liq., **246** (2017) 112-118.
10. M. Gopiraman, N. Selvakumaran, D. Kesavan, I.S. Kim, R. Karvembu, Ind. Eng. Chem. Res., **51** (2012) 7910-7922.
11. A. Dutta, S.S. Panja, M.M. Nandi, D. Sukul, J. Chem. Sci., **127** (2015) 921-929.
12. R. Solmaz, E.A. Sahin, A. Doner, G. Kardas, Corros. Sci., **53** (2011) 3231-3240.
13. O.K. Abiola, N.C. Oforka, Mater. Chem. Phys., **83** (2004) 315-322.
14. C. Jeyaprabha, S. Sathiyanarayanan, K.L.N. Phani, G. Venkatachari, Appl. Surf. Sci., **252** (2005) 966-975.
15. H. Okuda, Y. Koyama, T. Kojima, T. Takata, J. Polym. Sci., Part A: Polym. Chem., **51** (2013) 4541-4549.
16. G.S. Liou, H.J. Yen, Y.T. Su, H.Y. Lin, J Polym Sci Part A: Polym Chem., **45** (2007) 4352-4363.
17. H. Yeo, K. Tanaka, Y. Chujo, Polym., **60** (2015) 228-233.
18. X. Wang, F. Liu, J. Lai, Z. Fu, X. You, J. Fluorine Chem., **164** (2014) 27-37.
19. X. Xiong, X. Ma, P. Chen, L. Zhou, R. Ren, S. Liu, React. Funct. Polym., (2017) **https://doi.org/10.1016/j.reactfunctpolym.2017.12.017**
20. A. Iwan, E.S. Balcerzak, K.P. Korona, S. Grankowska, M. Kaminska, Synth. Met., **185-186** (2013) 17-24.

21. S. Hou, J. Zheng, S. Zhang, S. Li, Polym., **77** (2015) 48-54.
22. N. Gao, F. Zhang, S. Zhang, J. Liu, J. Membr. Sci., **372** (2011) 49-56.
23. J. Zheng, J. Wang, S. Zhang, T. Yuan, H. Yang, J. Power Sources., **245** (2014) 1005-1013.
24. S. Roy, S. Maiti, Polym., **39(16)** (1998) 3809-3813.
25. H. Jang, M.M. Islam, Y. Lim, S. Lee, M.A. Hossain, T. Hong, S. Lee, Y. Hong, W. Gi Kim, Solid State Ionics., **262** (2014) 845-851.
26. S.S. Vibhute, M.D. Joshi, P.P. Wadgaonkar, A.S. Patil, N.N. Maldar, J Polym Sci A: Polym Chem., **35** (1997) 3227-3234.
27. I. Fomenkov, I. V. Blagodatskikh, Iv. I. Ponomarev, Y.A. Volkovaa, I. I. Ponomarev, A. R. Khokhlov, Polym. Sci. Ser. B., **51(5-6)** (2009) 166-173.
28. H. Sun, C. Ma, B. Yuan, T. Wang, Y. Xu, Q. Xue, P. Li, Y. Kong, Sep. Purif. Technol., **122** (2014) 367-375.
29. P. Wen, Y. Kim, H. Chun, S.Y. Yang, M.H. Lee, Mater. Chem. Phys., **139** (2013) 923-930.
30. J.F. Blanco, Q.T. Nguyena, P. Schaetzel, J. Membr. Sci., **186** (2001) 267-279.
31. J. A. Desai, U. Dayal, P. H. Parsania, J. Macromol. Sci., A Pure Appl. Chem., **33(8)** (1996) 1113-1122.
32. P. Zhang, W. Linbo, L. Bo-Geng, Polym. Degrad. Stab., **94(8)** (2009) 1261-1266.
33. S. Mallakpour, Z. Rafiee, Polym. J., **39** (2007) 1185-1192.
34. G. S. Liou, S. H. Hsiao, H. M. Huang, C. W. Chang, H. J. Yen, J. Polym. Res., **14(3)** (2007) 191-199.
35. G. S. Liou, S. H. Hsiao, H. M. Huang, C. W. Chang, Polym. J., **39** (2007) 448-457.
36. W. Davidsohn, B. R. Laliberte, C. M. Goddard, C. M. Henry, J. Organomet. Chem., **36** (1972) 283-291.
37. F. Higashi, N. Akiyama, I. Takahashi, T. Koyama, J. Polym. Sci., Polym. Chem. Ed., **22(11)** (2003) 3607-3610.
38. I.O. Arukalam, Carbohydr. Polym., **112** (2014) 291-299.
39. A.M. Alsabagh, M.A. Migahed, H.S. Awad, Corros. Sci., **48** (2006) 813-828.
40. H. Hamani, T. Douadi, D. Daoud, M.A. Noaimi, S. Chafaa, Meas., **94** (2016) 837-846.
41. T.K. Chaitra, K.N. Mohana, D.M. Gurudatt, H.C. Tandon, J. Taiwan. Inst. Chem. E., **67** (2016) 521-531.
42. M.A. Deyab, A.E. Rehim, Int. J. Electrochem. Sci., **8** (2013) 12613-12627.
43. M.H. Hussin, A.A. Rahim, M.N.M. Ibrahim, N. Brosse, Meas., **78** (2016) 90-103.

44. S.A. Umoren, U.M. Eduok, M.M. Solomon, A.P. Udoh, Arabian J. Chem., **9** (2016) 209-224.
45. M.M. Solomon, S.A. Umoren, J. Environ. Chem. Eng., **3(3)** (2015) 1-15.
46. Y. Sangeetha, S. Meenakshi, C.S. Sundaram, Int. J. Biol. Macromol., **72** (2015) 1244-1249.
47. A.A. Farag, A.S. Ismail, M.A. Migahed, J. Mol. Liq., **211** (2015) 915-923.
48. F.M. Mahgoub, S.M. Al-Rashdi, OJPC., **6** (2016) 54-66.
49. Y. Sangeetha, S. Meenakshi, C.S. Sundaram, Carbohydr. Polym., **136** (2016) 38-45.
50. N. Soltani, N. Tavakkoli, M. Ghasemi, Int. J. Electrochem. Sci., **11** (2016) 8827-8847.
51. M.M. Solomon, S.A. Umoren, J. Colloid Interface Sci., **462** (2016) 29-41.
52. A. Pal, S. Dey, D. Sukul, Res. Chem. Interm., **42** (2016) 4531-4549.
53. G. Madhusudhana, R. Jaya Santhi, Int. J. Sci. Res., **4(1)** (2015) 1645-1650.
54. G. Karthik, M. Sundaravadivelu, Egypt. J. Pet., **25** (2016) 183-191.
55. P. Singh, A. Singh, M.A. Quiraishi, Res. Chem. Intermed.**, 40(2)** (2014) 595-604.
56. P.A. Lozada, O.O. Xometl, D.G. Lucero, N.V. Likhanova, M.A.D. Aguilar, I.V. Lijanaova, E.A. Estrada, Mater., **7** (2014) 5711-5734.
57. A. Jamal, M. Nasser, M.A. Sathiq, Arabian J. Chem., **9** (2016) 691-698.
58. A. Rasha, A. Ahmed, R.A. Farghali, A.M. Fekry, Int. J. Electrochem. Sci., **7** (2012) 7270-7282.
59. M.G. Sethuraman, V. Aishwarya, C. Kamal, T. Jebakumar, I. Edison, Arabian J. Chem., **10** (2017) 522--530.
60. K. Zakaria, A. Hamdy, M.A. Abbas, O.M. Abo-Elenien, J. Taiwan. Inst. Chem. E., **65** (2016) 530-543.
61. E.S. Ferreira, C. Giancomlli, F.C. Giacomlli, A. Spinelli, Mater. Chem. Phys., **83** (2004) 129-134.

Table 4.1 Inhibition efficiencies of various concentrations of the aromatic polyesters for corrosion of mild steel in 0.5 M H_2SO_4 obtained by weight loss measurement at ± 303 K

Name of the Inhibitor	Conc. (ppm)	Weight loss (g)	Inhibition Efficiency (%)	Surface Coverage (θ)	Corrosion rate (g cm^{-2} hr^{-1})
Blank	-		-	-	19.97
MPOB	10	0.1011	49.83	0.4983	10.02
	50	0.0950	52.84	0.5284	9.42
	100	0.0883	56.19	0.5619	8.75
	500	0.0499	75.26	0.7526	4.94
	1000	0.0405	79.88	0.7988	4.02
	1500	0.0502	75.11	0.7511	4.97
MPOP	10	0.0929	53.92	0.5392	9.20
	50	0.0907	54.98	0.5498	8.99
	100	0.0842	58.23	0.5823	8.34
	500	0.0493	75.51	0.7551	4.89
	1000	0.0364	81.92	0.8192	3.61
	1500	0.0479	76.24	0.7624	4.74
MPOHX	10	0.0905	55.11	0.5511	8.96
	50	0.0849	57.85	0.5785	8.42
	100	0.0799	60.33	0.6033	7.92
	500	0.0445	77.93	0.7793	4.41
	1000	0.0359	82.2	0.822	3.55
	1500	0.0424	78.95	0.7895	4.20
MPOHP	10	0.0868	56.91	0.5691	8.60
	50	0.0823	59.14	0.5914	8.16
	100	0.0768	61.89	0.6189	7.61
	500	0.0435	78.43	0.7843	4.31
	1000	0.0313	84.48	0.8448	3.10
	1500	0.0376	81.36	0.8136	3.72
MPOO	10	0.0821	59.24	0.5924	8.14
	50	0.0755	62.52	0.6252	7.48

	100	0.0690	65.75	0.6575	6.84
	500	0.0428	78.78	0.7878	4.24
	1000	0.0269	86.67	0.8667	2.66
	1500	0.0299	85.15	0.8515	2.96
MPON	10	0.0761	62.23	0.6223	7.54
	50	0.0703	65.09	0.6509	6.97
	100	0.0608	69.83	0.6983	6.02
	500	0.0366	81.85	0.8185	3.62
	1000	0.0187	90.72	0.9072	1.85
	1500	0.0256	87.29	0.8729	2.53
MPOD	10	0.0698	65.36	0.6536	6.92
	50	0.0610	69.71	0.6971	6.05
	100	0.0559	72.24	0.7224	5.54
	500	0.0329	83.69	0.8369	3.26
	1000	0.0164	91.85	0.9185	1.63
	1500	0.0261	87.04	0.8704	2.58
MPOU	10	0.0624	69.04	0.6904	6.18
	50	0.0536	73.4	0.734	5.31
	100	0.0480	76.19	0.7619	4.75
	500	0.0201	90.01	0.9001	1.99
	1000	0.0141	92.98	0.9298	0.76
	1500	0.0219	89.15	0.8915	2.16

Table 4.2 Inhibition efficiencies of selected concentrations of the aromatic polyesters for corrosion of mild steel in 0.5 M H_2SO_4 obtained by weight loss measurement at higher temperature

Name of the inhibitor	Conc. (ppm)	303 K		313 K		323 K		333 K	
		IE (%)	CR (g cm^{-2} hr^{-1})	IE (%)	CR (g cm^{-2} hr^{-1})	IE (%)	CR (g cm^{-2} hr^{-1})	IE (%)	CR (g cm^{-2} hr^{-1})
Blank	-	-	17.39	-	80.13	-	102.01	-	122.34
MPOB	10	38.80	10.64	34.26	52.67	31.95	69.42	30.58	84.93
	100	48.55	8.95	46.65	42.75	43.28	57.86	40.91	72.29
	1000	71.79	4.91	62.19	30.30	55.41	45.49	50.34	60.76
MPOP	10	41.54	10.17	37.11	50.39	33.57	67.76	32.24	82.90
	100	49.57	8.77	46.82	42.61	42.13	59.03	41.59	71.46
	1000	80.34	3.42	72.13	22.33	65.58	35.11	58.39	50.91
MPOHX	10	46.15	9.37	40.15	47.96	35.62	65.67	33.38	81.51
	100	51.11	8.50	47.56	42.02	44.75	56.36	42.57	70.26
	1000	81.71	3.18	75.29	19.80	70.31	30.29	63.12	45.12
MPOHP	10	50.26	8.65	44.63	44.37	42.51	58.64	37.46	76.51
	100	58.80	7.17	51.71	38.69	47.06	54.00	44.39	68.04
	1000	82.91	2.97	78.61	17.14	74.09	26.43	71.29	35.13
MPOO	10	53.68	8.06	48.09	41.59	45.68	55.41	41.93	71.05
	100	59.83	6.99	55.82	35.40	52.08	48.88	49.52	61.76
	1000	84.44	2.71	81.43	14.88	78.21	22.23	75.14	30.41
MPON	10	54.70	7.88	51.71	38.69	48.02	53.02	44.34	68.10
	100	62.91	6.45	57.39	34.14	56.32	44.56	52.21	58.47
	1000	86.67	2.32	84.11	12.73	80.05	20.35	77.31	27.76
MPOD	10	59.66	7.02	55.27	35.84	51.95	49.02	48.67	62.80
	100	64.44	6.18	61.08	31.19	59.32	41.50	55.16	54.86
	1000	89.57	1.81	86.35	10.94	83.57	16.76	81.2	23.00
MPOU	10	63.08	6.42	60.57	31.59	54.23	46.69	52.71	57.86
	100	65.98	5.92	63.36	29.36	60.53	40.26	57.31	52.23
	1000	91.11	1.55	88.82	8.96	85.26	15.04	83.65	20.00

Table 4.3 Activation parameters for mild steel corrosion in 0.5 M H_2SO_4 calculated by Arrhenius, Transition State and basic thermodynamic equations

Name of the inhibitor	E_a kJ/ mol	ΔH^o kJ /mol	ΔS^o kJ/mol/ K	Heat of adsorption (Q)	ΔG^o (kJ / mol)			
					303K	313K	323K	333K
Blank	51.81	49.17	-55.99	-	17.02	17.57	18.13	18.69
MPOB	67.53	64.89	-14.23	-25.4657	4.39	4.53	4.68	4.82
MPOP	72.52	69.89	-10.53	-29.4865	2.64	2.73	2.81	2.90
MPOHX	71.04	68.41	-6.47	-26.2315	2.02	2.09	2.15	2.22
MPOHP	63.84	61.21	-30.17	-15.7006	9.20	9.50	9.81	10.11
MPOO	64.98	62.35	-27.95	-16.275	8.53	8.81	9.09	9.37
MPON	67.12	64.48	-22.23	-18.5727	6.80	7.02	7.25	7.46
MPOD	68.28	65.64	-20.20	-19.1471	6.18	6.39	6.59	6.79
MPOU	69.55	66.91	-17.49	-20.1045	5.36	5.54	5.72	5.89

Table 4.4 Various Adsorption isotherm parameters for mild steel in 0.5 M H_2SO_4 containing various concentrations of aromatic polyesters at room temperature

Name of the inhibitor	Langmuir		Temkin		El-Awady		Flory Huggins	
	R^2	$-\Delta G^{\circ}_{ads}$ kJ mol^{-1}	R^2	$-\Delta G^{\circ}_{ads}$ kJ mol^{-1}	R^2	$-\Delta G^{\circ}_{ads}$ kJ mol^{-1}	R^2	$-\Delta G^{\circ}_{ads}$ kJ mol^{-1}
MPOB	0.9981	36.42	0.8705	24.38	0.8561	10.63	0.7986	26.39
MPOP	0.9974	36.39	0.8258	24.77	0.8073	10.55	0.7467	26.10
MPOHX	0.9986	35.94	0.8615	24.94	0.8433	10.59	0.7934	25.40
MPOHP	0.9979	36.03	0.8531	25.27	0.8259	9.92	0.7713	25.67
MPOO	0.9969	35.88	0.8871	25.53	0.8339	9.88	0.7758	25.18
MPON	0.9965	35.77	0.8883	25.68	0.8053	9.73	0.7425	26.13
MPOD	0.9971	35.41	0.9039	25.71	0.8063	10.01	0.7496	25.47
MPOU	1.03	35.01	0.9151	25.87	0.7946	10.52	0.7456	26.77

Table 4.5 Thermodynamic parameters for mild steel corrosion in 0.5 M H_2SO_4 at different temperatures calculated from van't Hoff and Gibbs Helmholtz equation

Name of the inhibitor	Van't Hoff equation		Gibbs-Helmholtz equation	$-\Delta G^{\circ}_{ads}$ kJ mol^{-1}			
	ΔH°_{ads} kJ mol^{-1}	ΔS°_{ads} kJ mol^{-1}	ΔH°_{ads} kJ mol^{-1}	303 K	313 K	323 K	333 K
MPOB	-25.64	0.0135	-25.64	-29.88	-29.73	-29.92	-30.29
MPOP	-29.53	0.0047	-29.53	-31.07	-30.91	-31.07	-31.19
MPOHX	-26.29	0.0164	-26.29	-31.30	-31.33	-31.66	-31.74
MPOHP	-15.74	0.0511	-15.74	-31.18	-31.82	-32.16	-32.77
MPOO	-16.45	0.0506	-16.45	-31.79	-32.28	-32.77	-33.31
MPON	-18.59	0.0451	-18.59	-32.24	-32..77	-33.08	-33.64
MPOD	-19.21	0.0450	-19.21	-32.94	-33.23	-33.71	-34.30
MPOU	-20.23	0.0433	-20.23	-33.39	-33.83	-34.05	-34.77

Table 4.6 AC-impedance parameters for the corrosion of mild steel for selected concentrations of the aromatic polyesters in 0.5 M H_2SO_4

Name of the inhibitor	Conc. (ppm)	R_{ct} (ohm cm^2)	C_{dl} (µF/cm^2)	Inhibition efficiency (%)
BLANK	-	15.8	66.7	-
MPOB	10	24.93	41.1	36.62
	100	27.01	32.1	41.50
	1000	41.79	27.1	62.19
MPOP	10	27.01	47.9	41.50
	100	27.77	40.6	43.10
	1000	51.39	33.4	69.25
MPOHX	10	27.31	49.9	42.15
	100	30.69	35.6	48.52
	1000	52.45	31.9	69.88
MPOHP	10	30.02	41.6	47.37
	100	34.67	36.9	54.43
	1000	52.53	30.6	69.92
MPOO	10	31.16	42.2	49.29
	100	36.21	32	56.37
	1000	62.84	29.7	74.86
MPON	10	31.63	38.7	50.05
	100	39.73	26.4	60.23
	1000	76.73	22.1	79.41
MPOD	10	32.91	29.5	51.99
	100	46.14	18.3	65.76
	1000	88.76	16.7	82.20
MPOU	10	35.67	36.1	55.71
	100	49.95	23.1	68.37
	1000	101.86	19.2	84.49

Table 4.7 Potentiodynamic polarisation parameters for corrosion of mild steel with selected concentration of the aromatic polyesters in 0.5 M H_2SO_4

Name of the inhibitor	Conc. (ppm)	Tafel slopes (mV/dec)		$-E_{corr}$ (mV) vs SCE	I_{corr} ($\mu A/cm^2$)	Inhibition efficiency (%)
		b_a	b_c			
BLANK	-	63	153	476.9	896.52	-
MPOB	10	56	166	468.3	552.70	38.35
	100	58	172	465.9	451.76	49.61
	1000	45	173	464.2	322.03	64.08
MPOP	10	63	159	487.9	505.19	43.65
	100	54	152	479.3	472.91	47.25
	1000	51	149	478.8	284.11	68.31
MPOHX	10	52	151	479.7	436.78	51.28
	100	53	145	480	409.17	54.36
	1000	49	147	477.8	268.51	70.05
MPOHP	10	50	169	470	430.96	51.93
	100	51	173	469	382.90	57.29
	1000	44	176	464.6	236.50	73.62
MPOO	10	42	166	468.9	405.85	54.73
	100	47	157	474.6	376.00	58.06
	1000	44	159	471.3	211.67	76.39
MPON	10	46	166	471.7	382.63	57.32
	100	49	157	474.8	347.13	61.28
	1000	46	156	472	149.00	83.38
MPOD	10	64	165	473.1	364.88	59.30
	100	59	161	466.9	305.27	65.95
	1000	57	163	475.8	129.73	85.53
MPOU	10	54	164	476.3	360.31	59.81
	100	52	159	475.7	295.49	67.04
	1000	50	167	474.7	159.04	82.26

Table 4.8 Elemental composition from EDS analysis

Element (Wt %)	Uninhibited	MPOB inhibited	MPOU inhibited
C	2.43	42.5	51.8
O	31.58	24.35	19.09
Fe	64.87	32.10	27.77
S	1.12	1.05	1.34

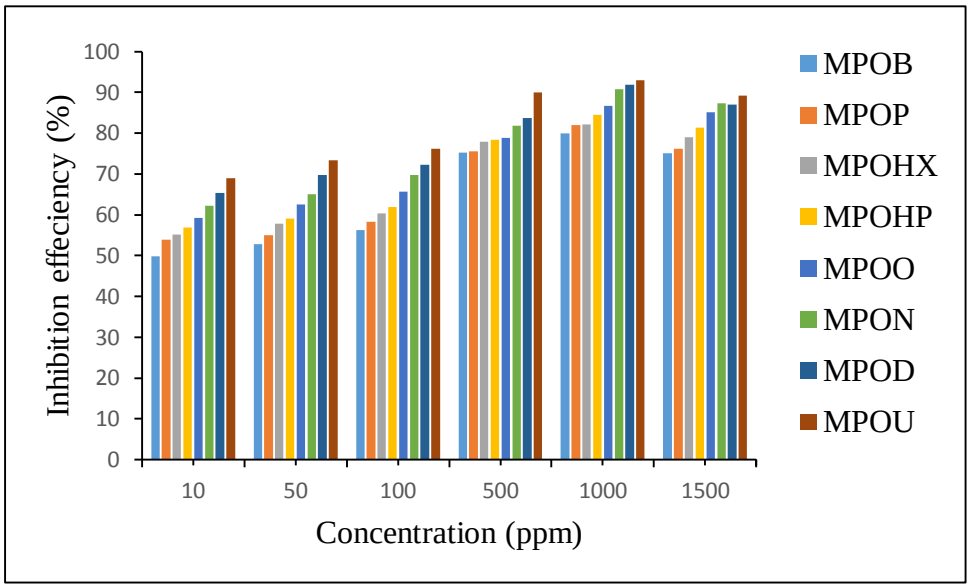

Fig. 4.1 Variation of Inhibition efficiency for selected concentrations of the aromatic polyesters in 0.5 M H_2SO_4

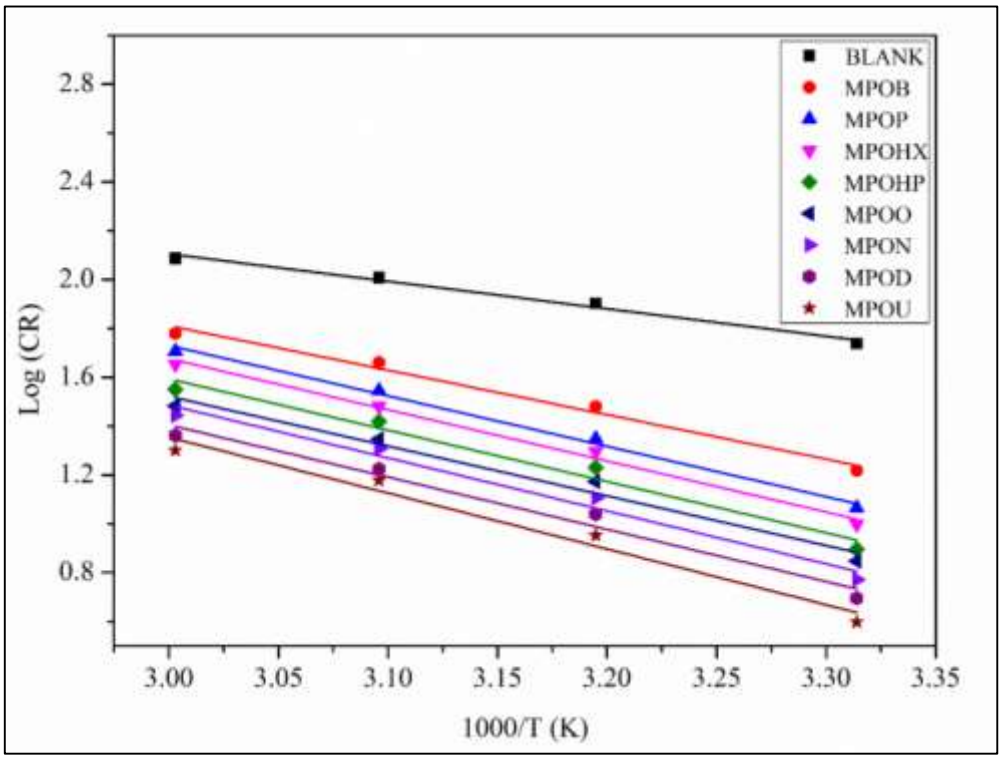

Fig. 4.2 Arrhenius plot for corrosion of mild steel in 0.5 M H_2SO_4 in the absence and presence of aromatic polyesters

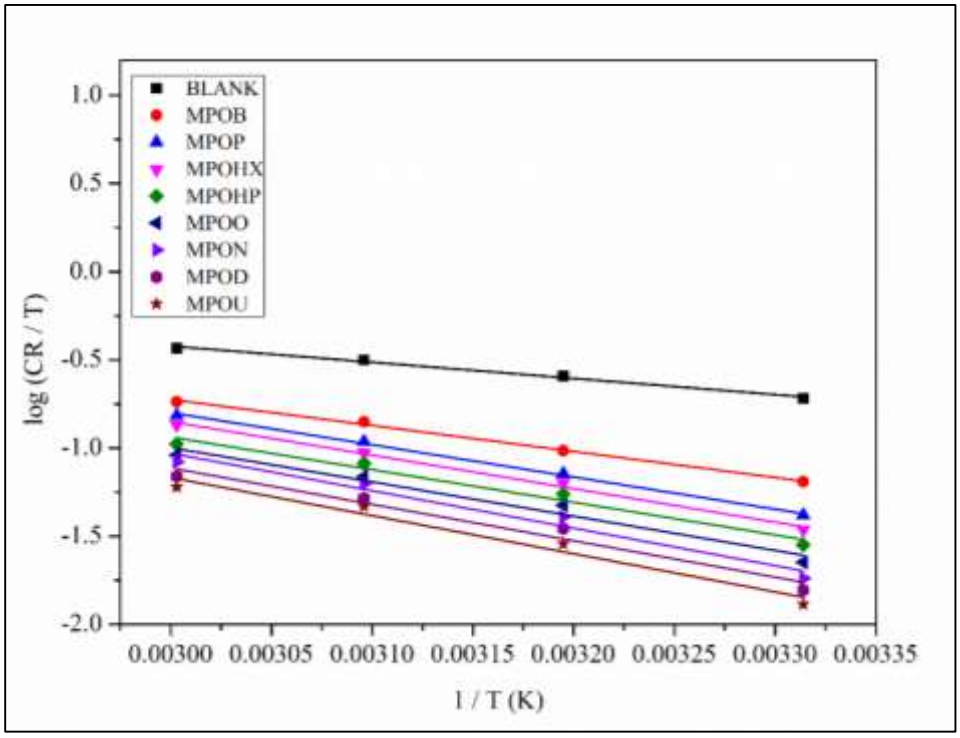

Fig. 4.3 Transition State plot of corrosion of mild steel in 0.5 M H_2SO_4 in the absence and presence of aromatic polyesters

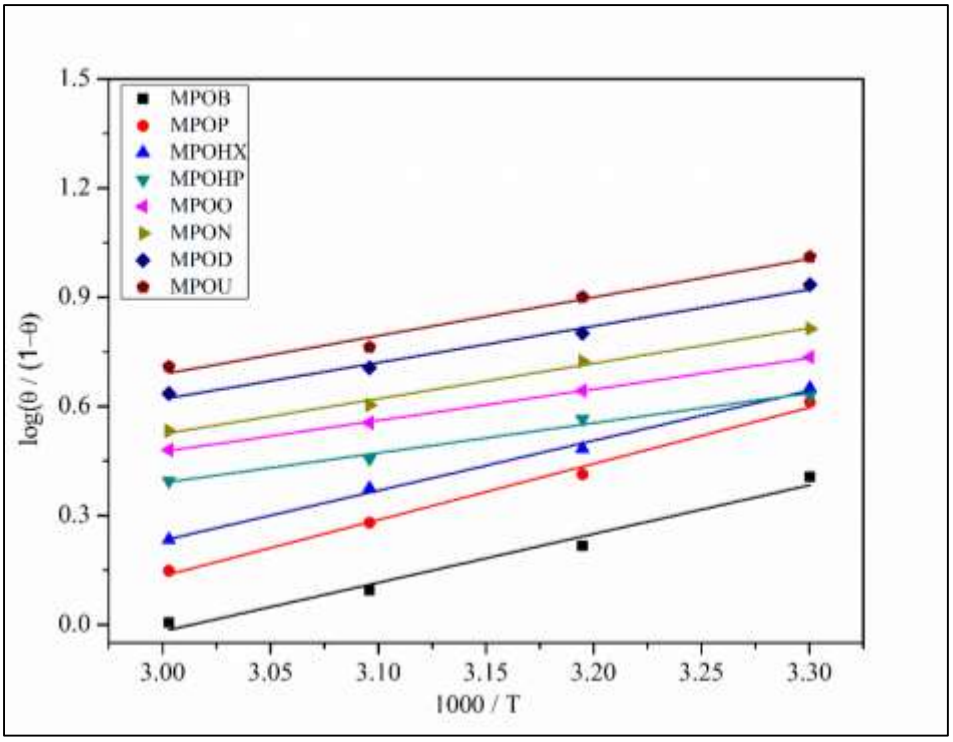

Fig. 4.4 Plot of log (Ɵ / 1- Ɵ) Vs 1000/T for mild steel in 0.5 M H_2SO_4 in the absence and presence of aromatic polyesters

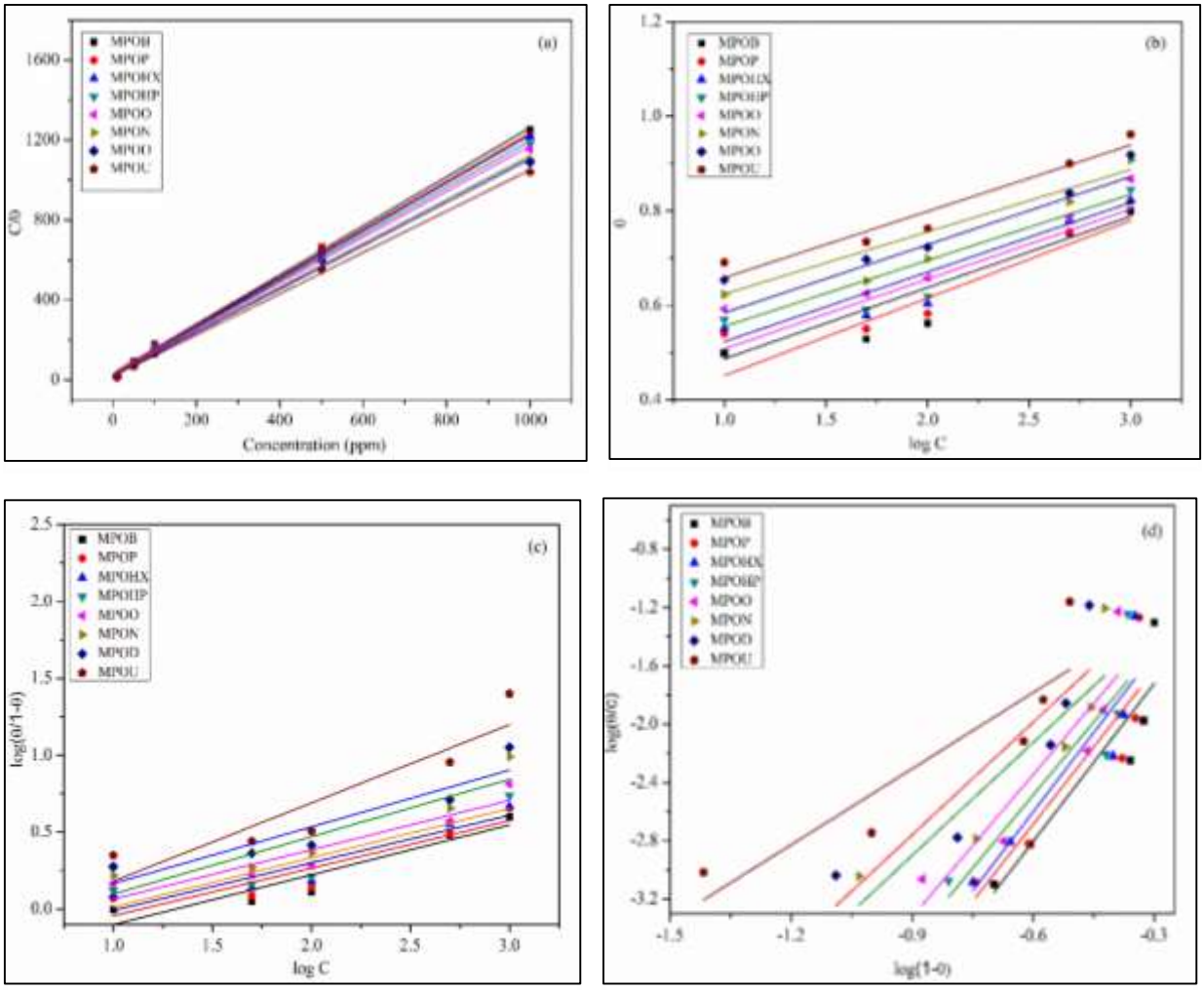

Fig. 4.5 Plots representing Adsorption isotherm models of a) Langmuir

b) Temkin c) El-Awady d) Flory-Huggins

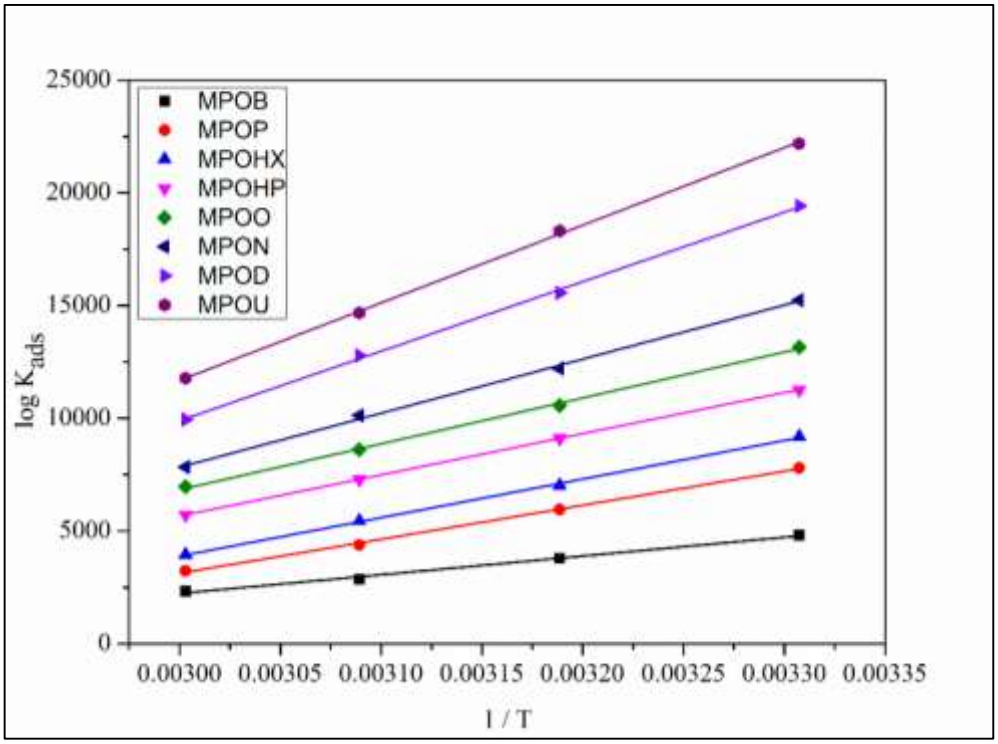

Fig. 4.6 The relationship between log K_{ads} and 1/T

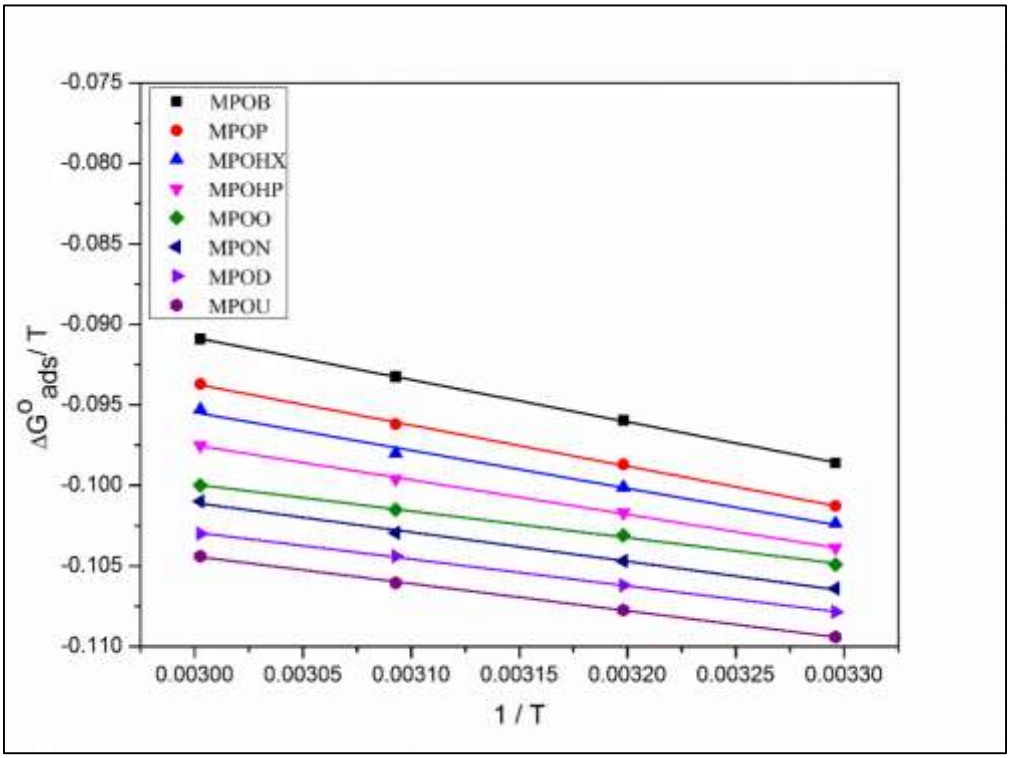

Fig. 4.7 The relationship between ΔG°_{ads}/T and 1/T

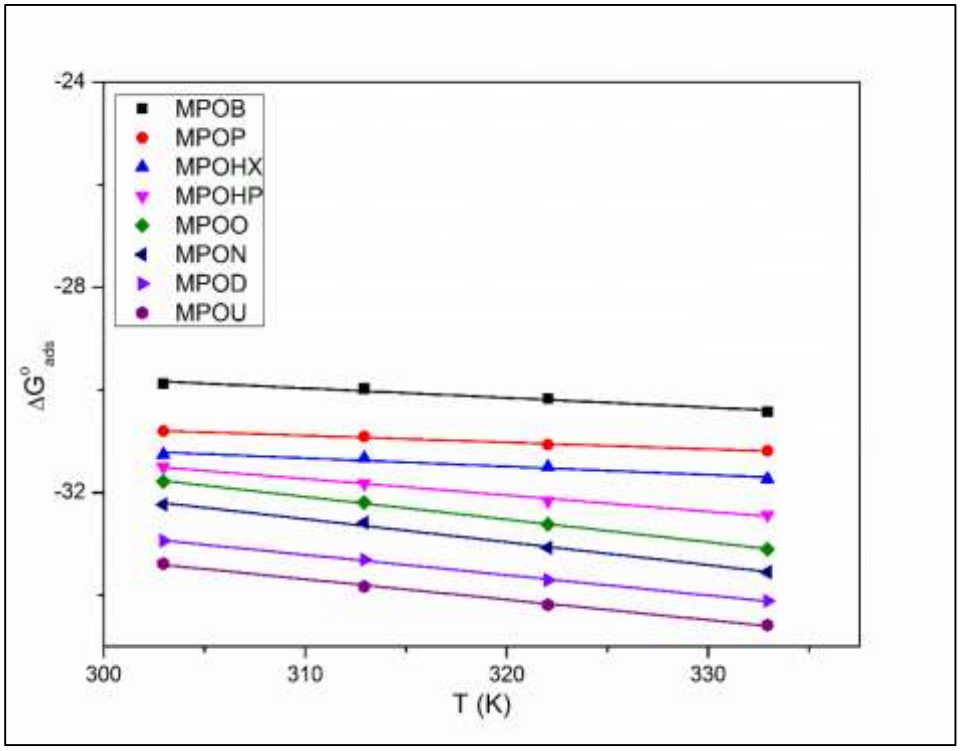

Fig. 4.8 The relationship between ΔG°_{ads} and T

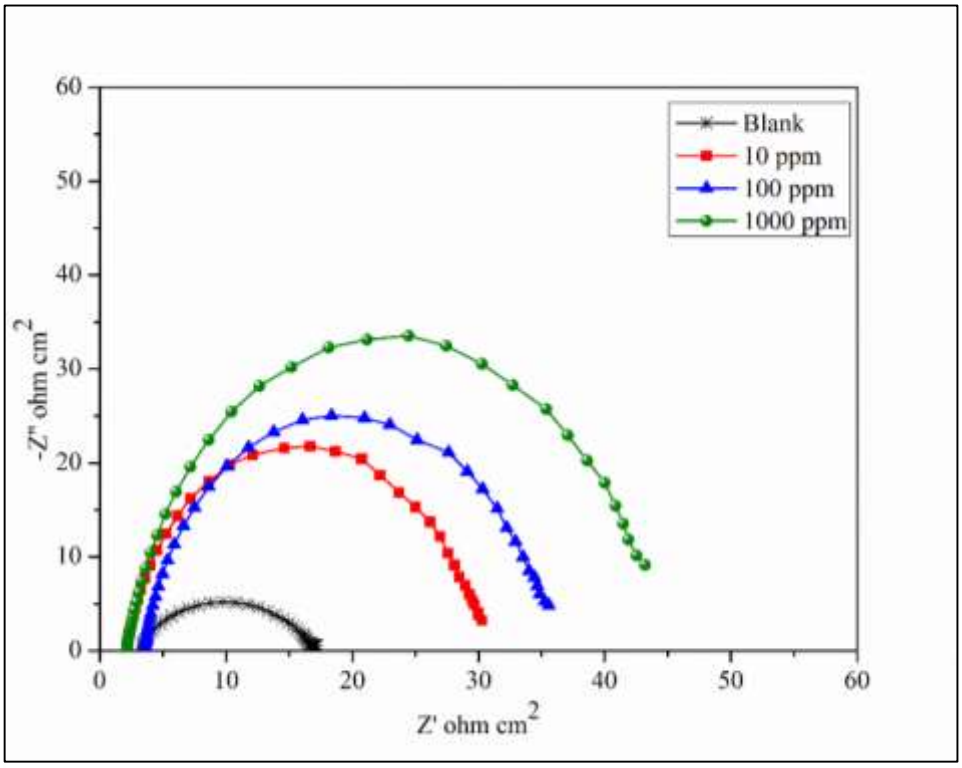

Fig. 4.9 Nyquist plot for mild steel in 0.5 M H_2SO_4 for selected concentrations of MPOB

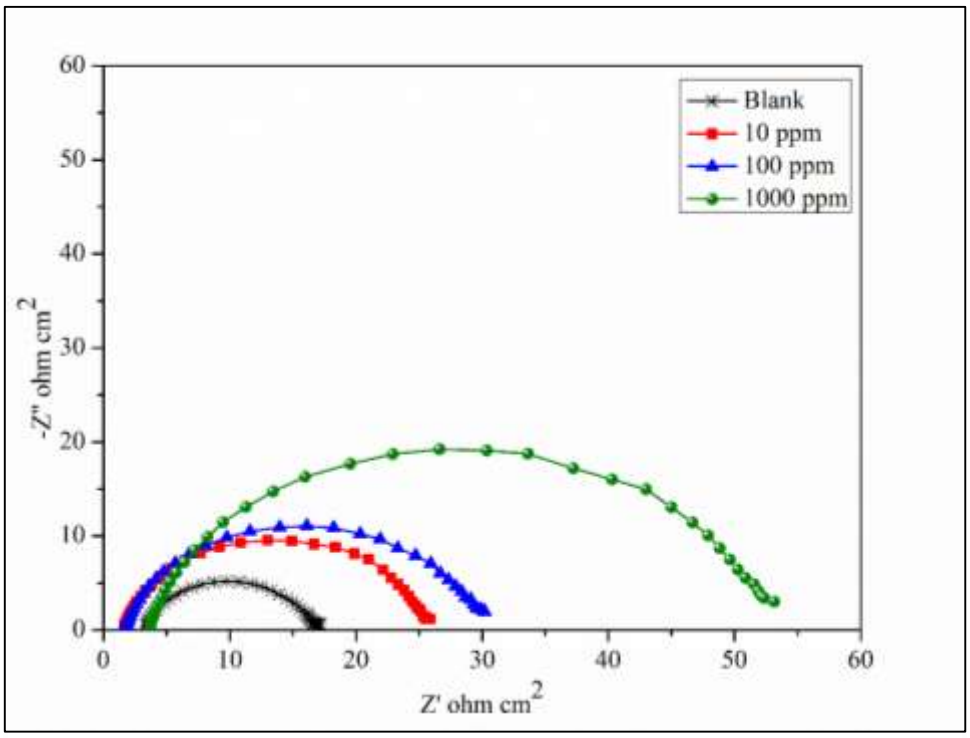

Fig. 4.10 Nyquist plot for mild steel in 0.5 M H_2SO_4 for selected concentrations of MPOP

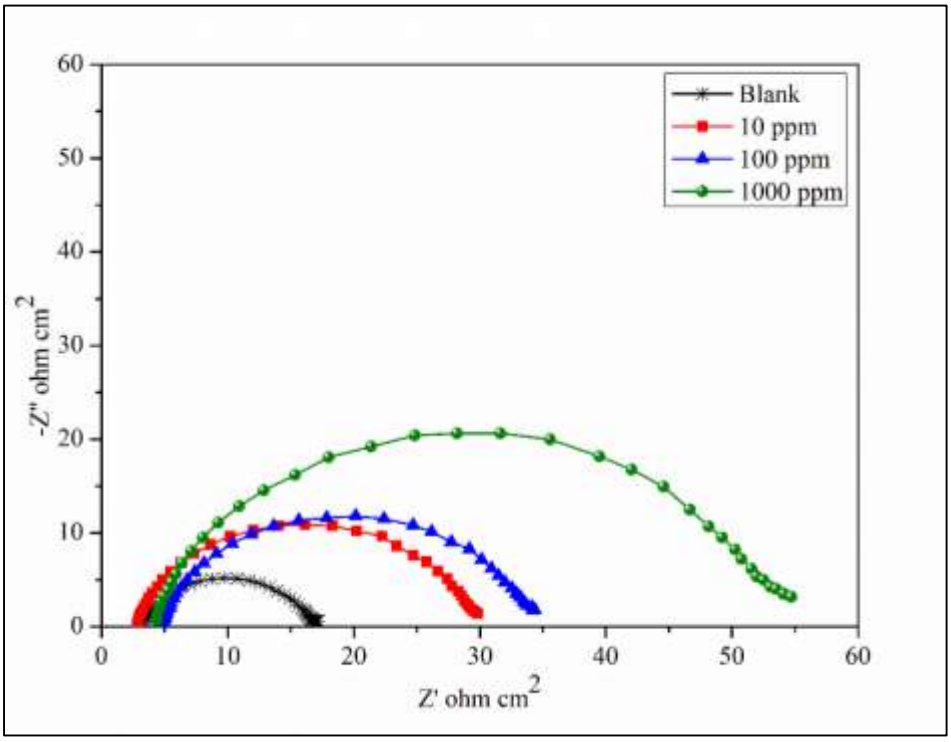

Fig. 4.11 Nyquist plot for mild steel in 0.5 M H_2SO_4 for selected concentrations of MPOHX

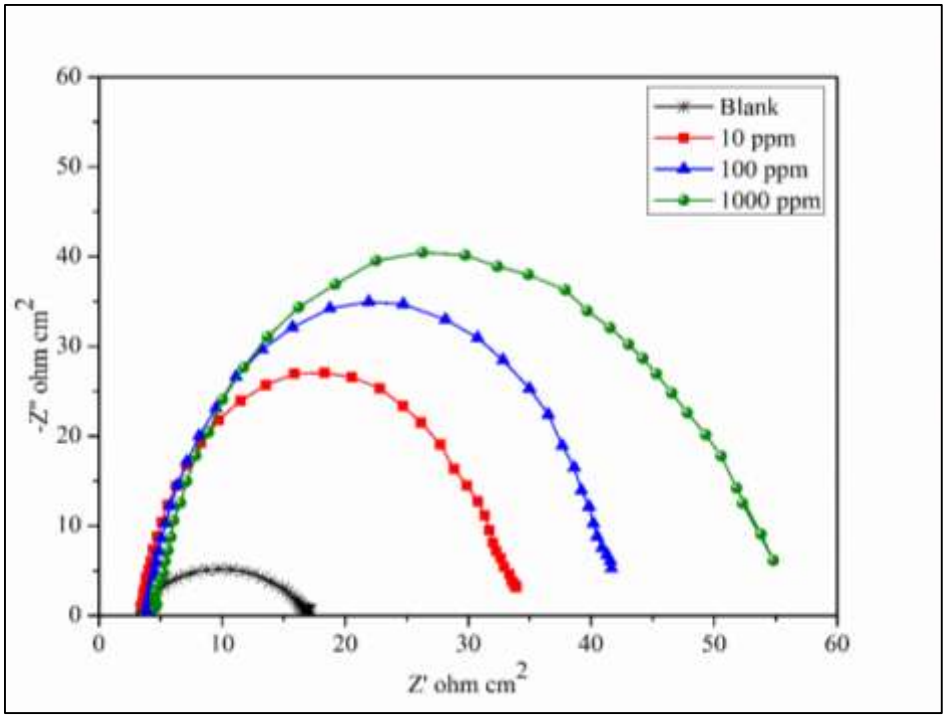

Fig. 4.12 Nyquist plot for mild steel in 0.5 M H_2SO_4 for selected concentrations of MPOHP

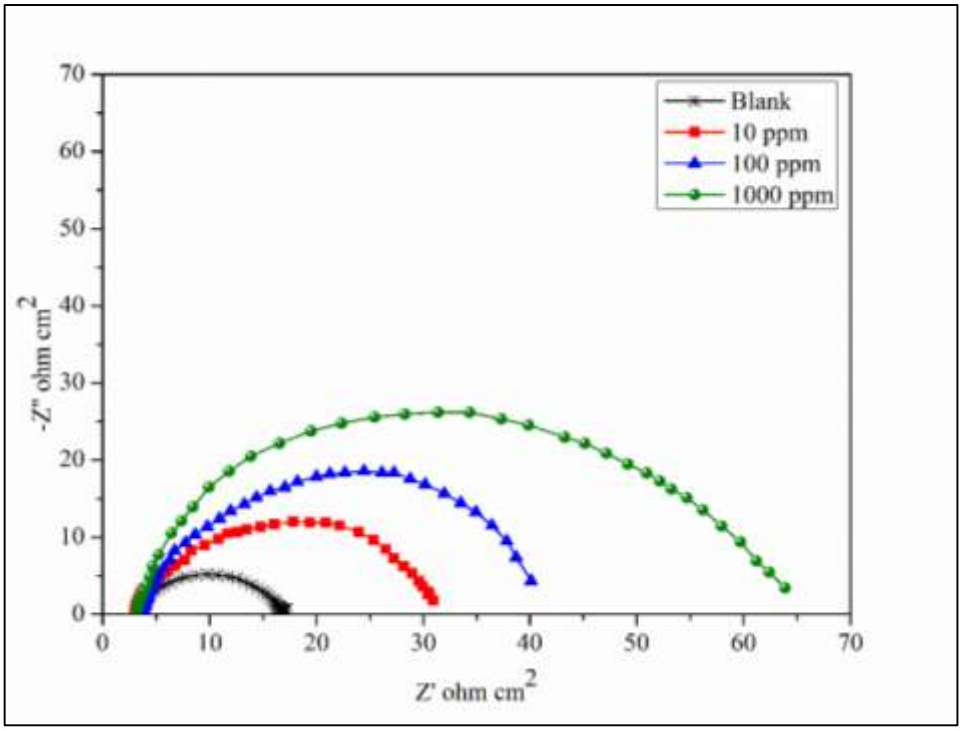

Fig. 4.13 Nyquist plot for mild steel in 0.5 M H_2SO_4 for selected concentrations of MPOO

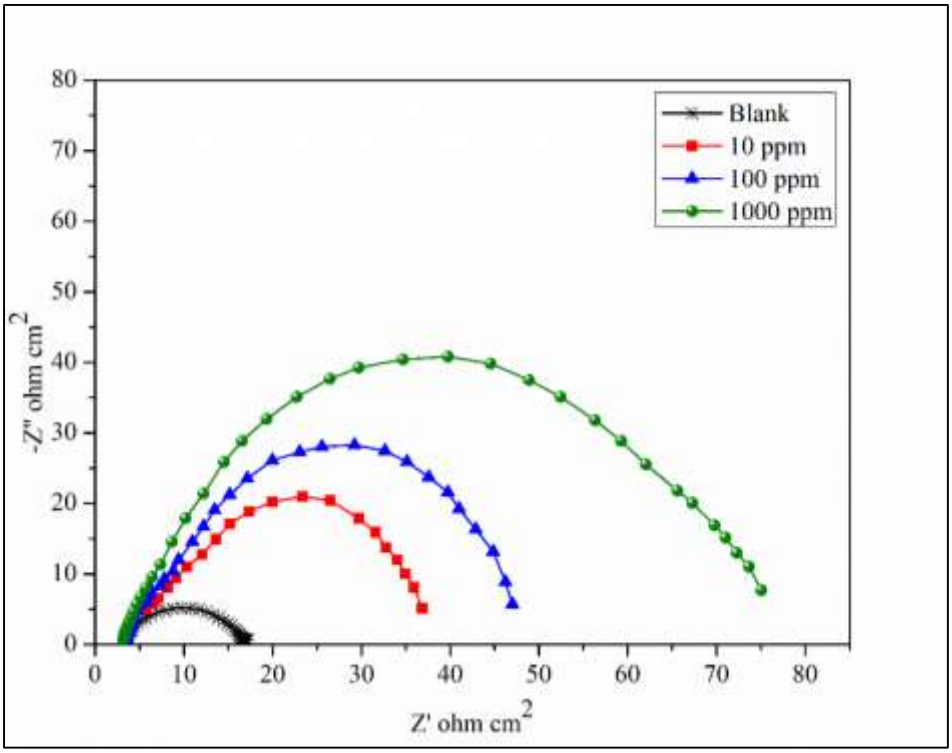

Fig. 4.14 Nyquist plot for mild steel in 0.5 M H_2SO_4 for selected concentrations of MPON

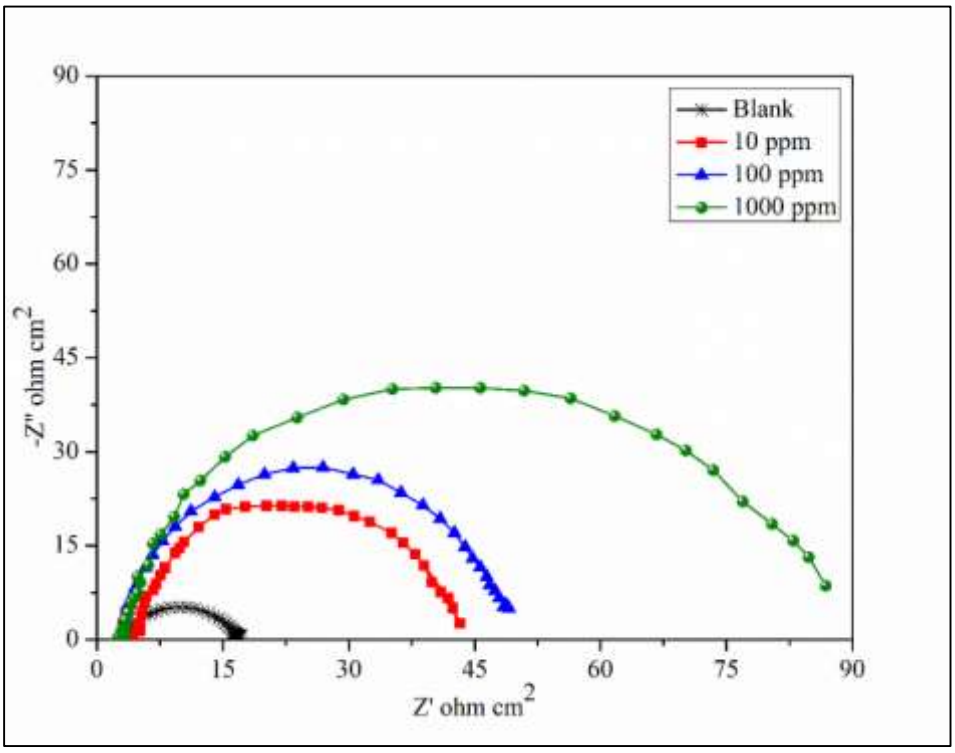

Fig. 4.15 Nyquist plot for mild steel in 0.5 M H_2SO_4 for selected concentrations of MPOD

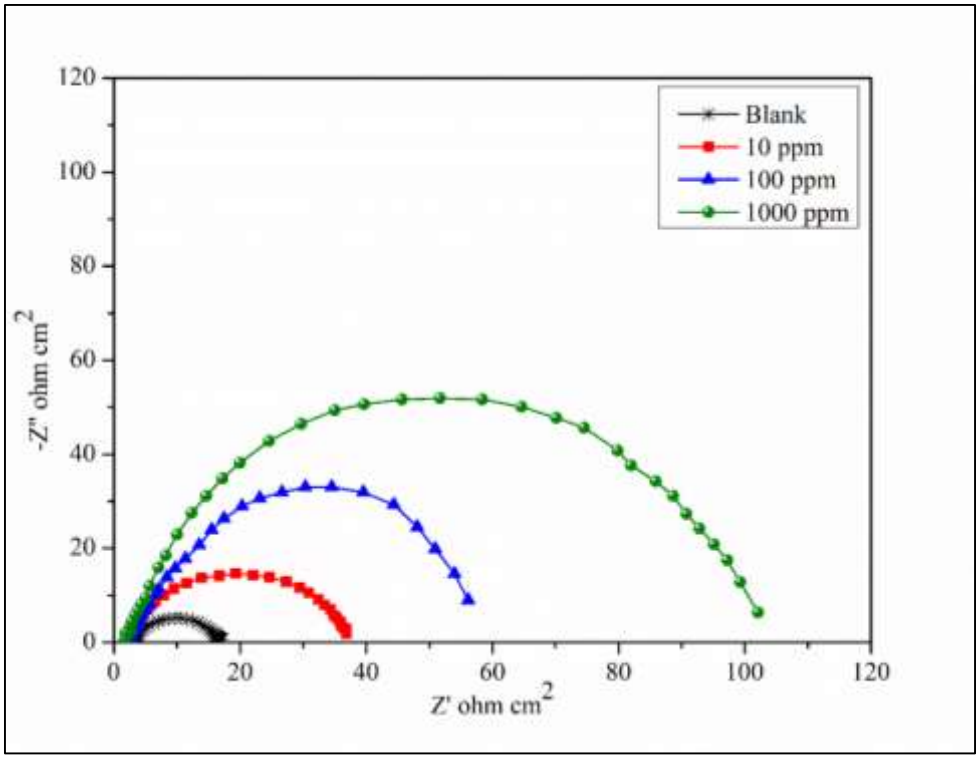

Fig. 4.16 Nyquist plot for mild steel in 0.5 M H_2SO_4 for selected concentrations of MPOU

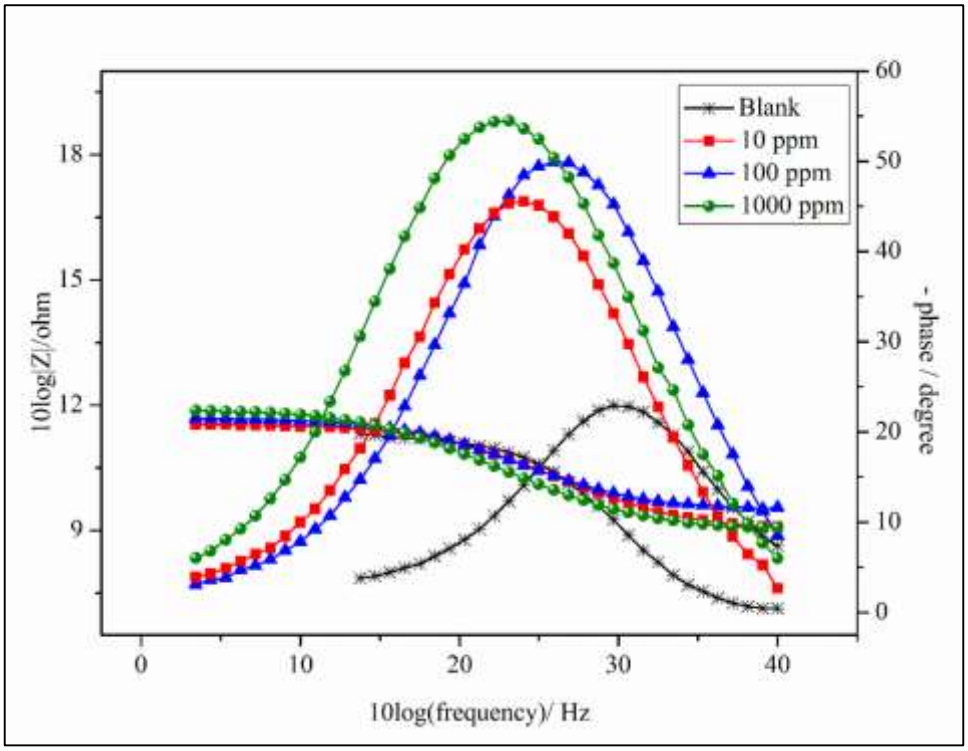

Fig. 4.17 Bode plot for mild steel in 0.5 M H_2SO_4 for selected concentrations of MPOB

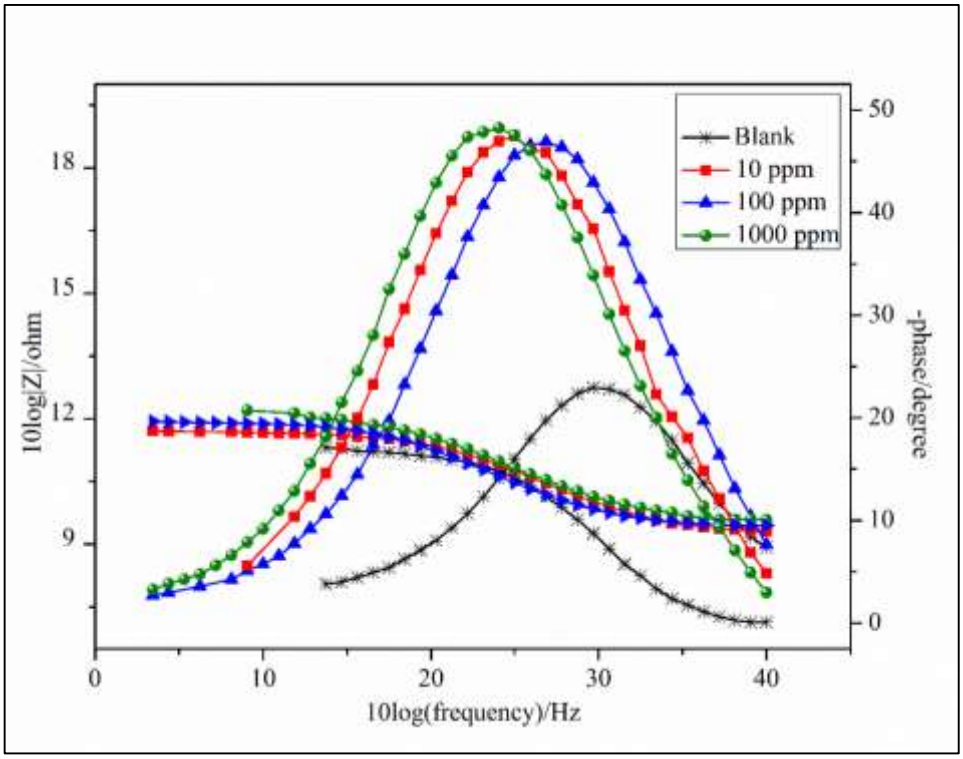

Fig. 4.18 Bode plot for mild steel in 0.5 M H_2SO_4 for selected concentrations of MPOP

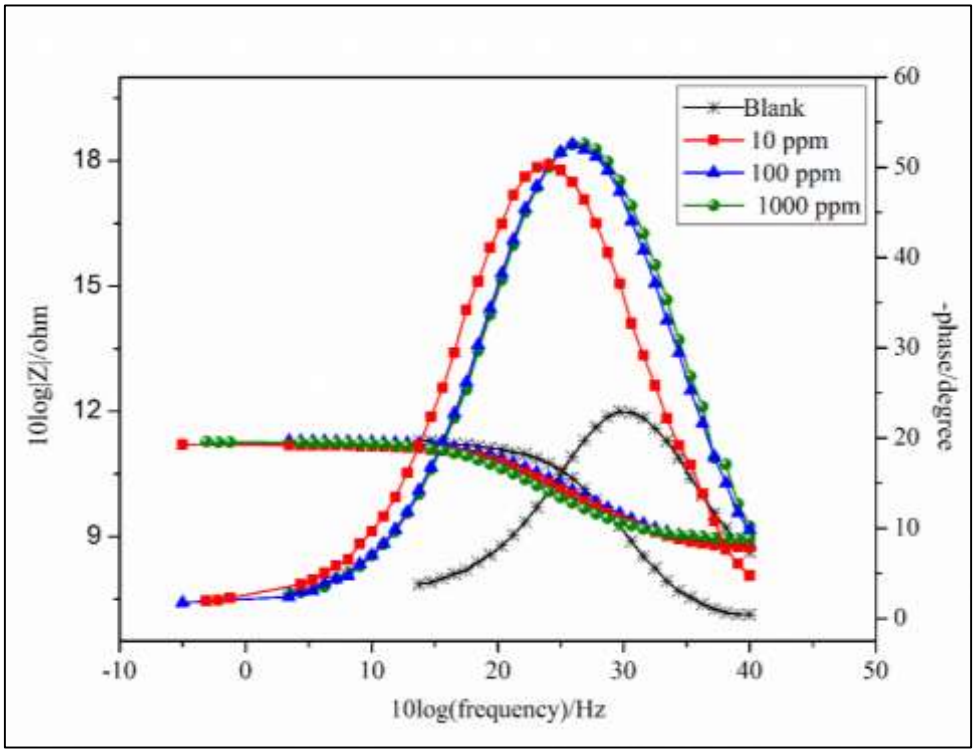

Fig. 4.19 Bode plot for mild steel in 0.5 M H_2SO_4 for selected concentrations of MPOHX

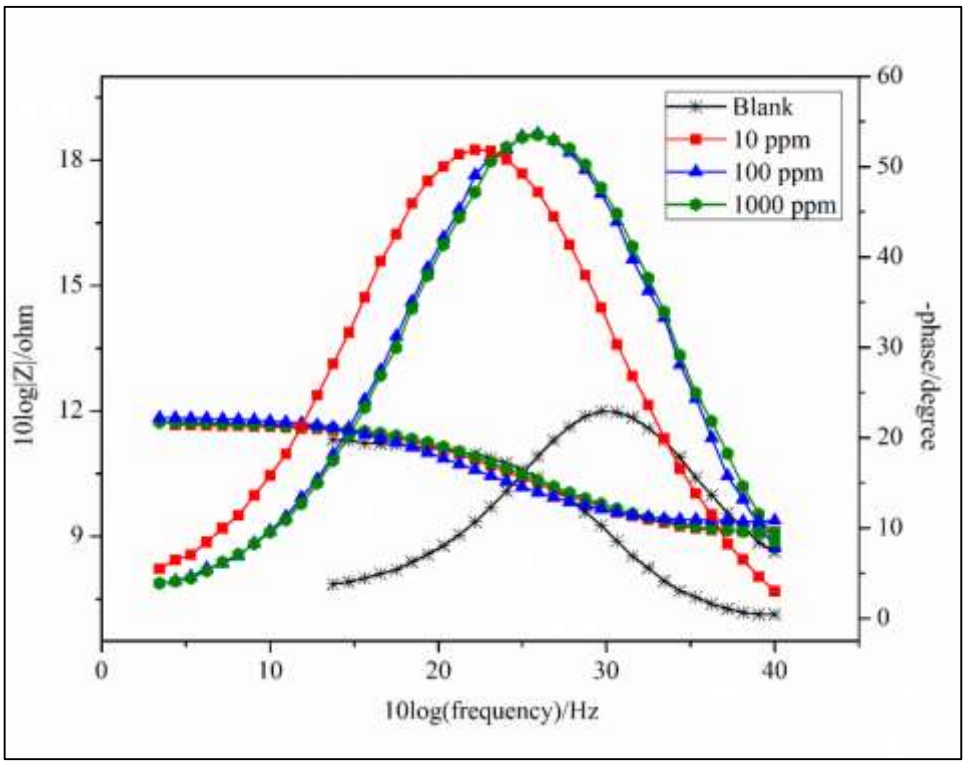

Fig. 4.20 Bode plot for mild steel in 0.5 M H_2SO_4 for selected concentrations of MPOHP

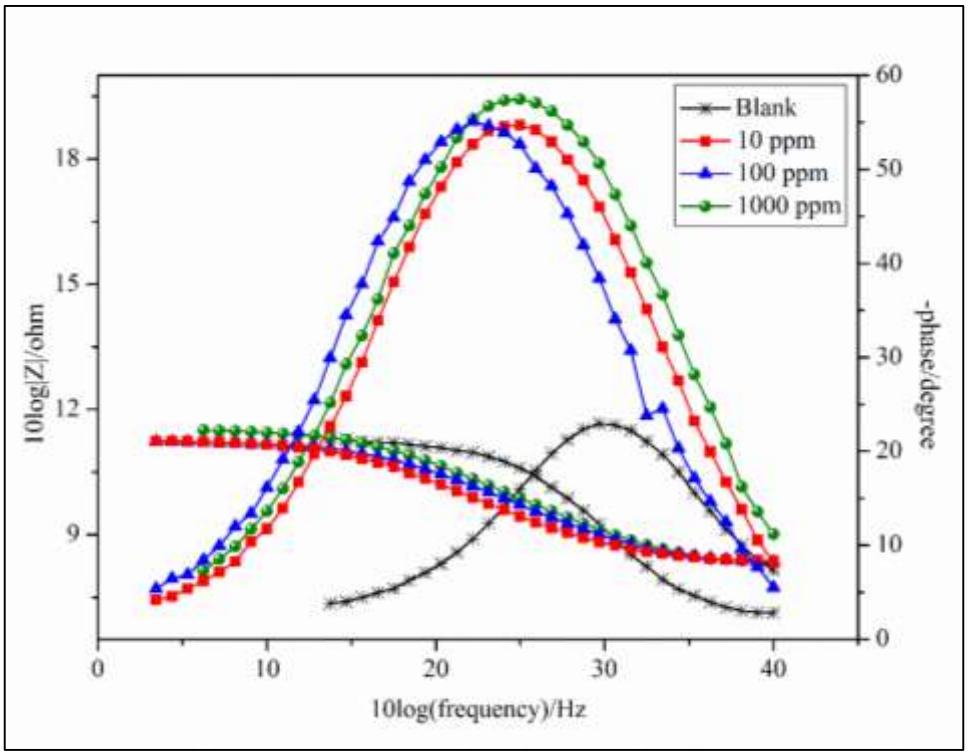

Fig. 4.21 Bode plot for mild steel in 0.5 M H_2SO_4 for selected concentrations of MPOO

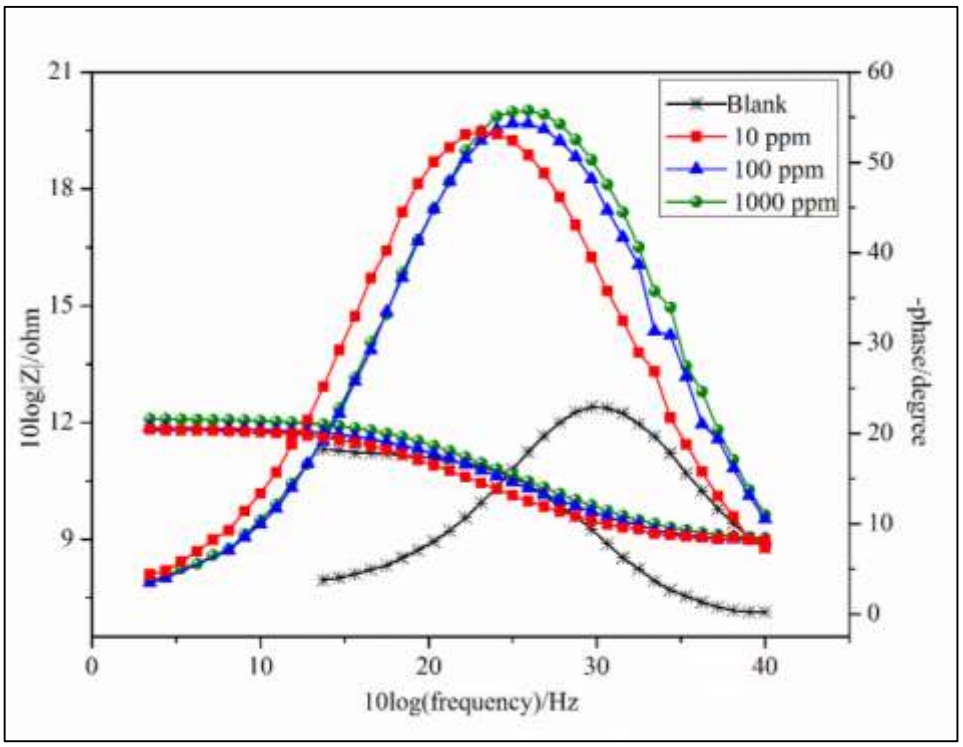

Fig. 4.22 Bode plot for mild steel in 0.5 M H_2SO_4 for selected concentrations of MPON

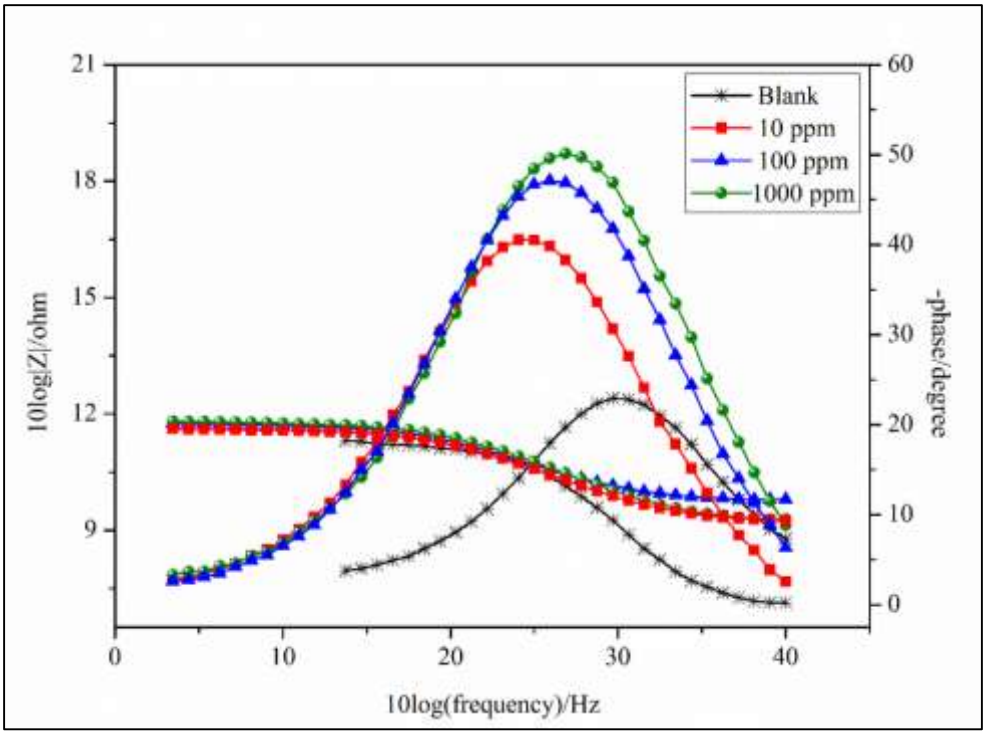

Fig. 4.23 Bode plot for mild steel in 0.5 M H_2SO_4 for selected concentrations of MPOD

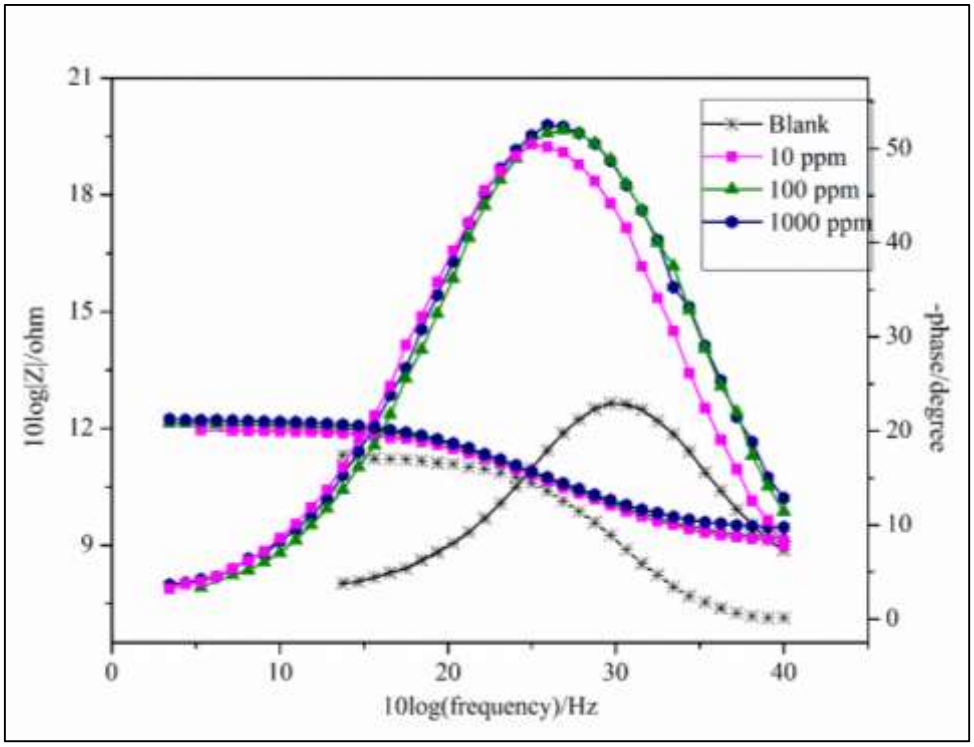

Fig. 4.24 Bode plot for mild steel in 0.5 M H_2SO_4 for selected concentrations of MPOU

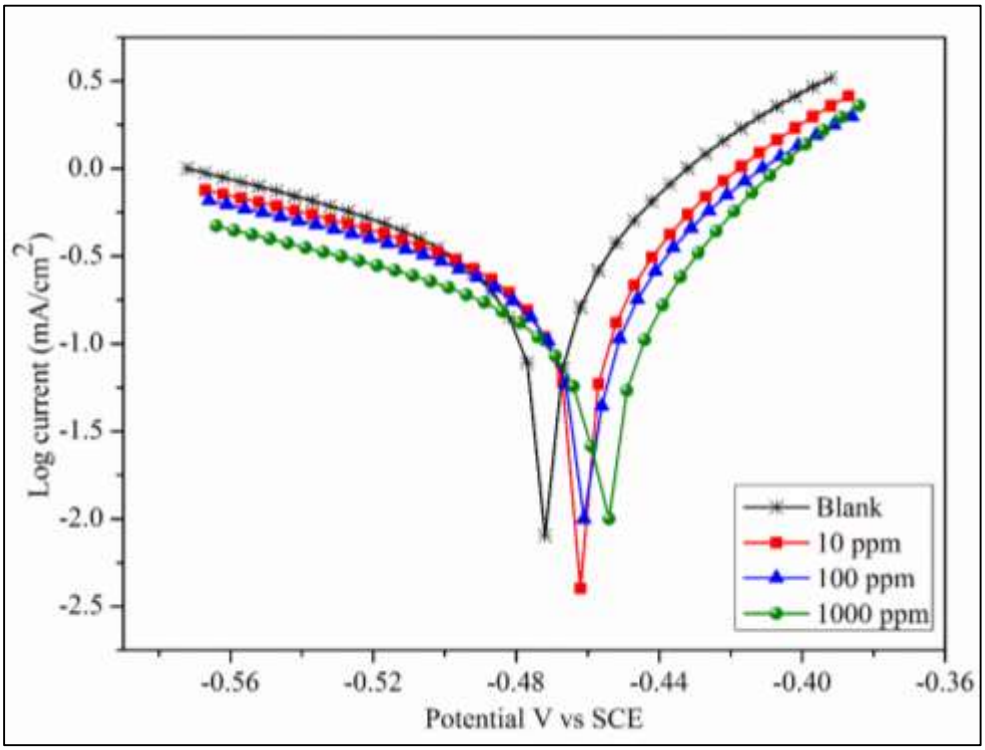

Fig. 4.25 Polarization curves for mild steel 0.5 M H_2SO_4 for selected concentrations of MPOB

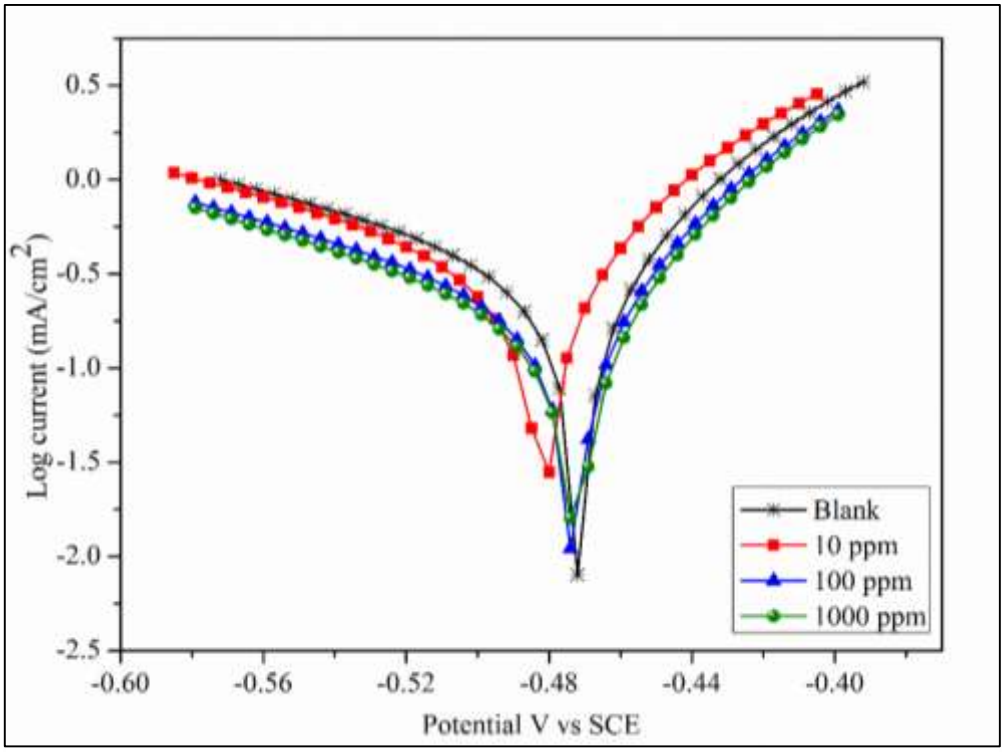

Fig. 4.26 Polarization curves for mild steel 0.5 M H_2SO_4 for selected concentrations of MPOP

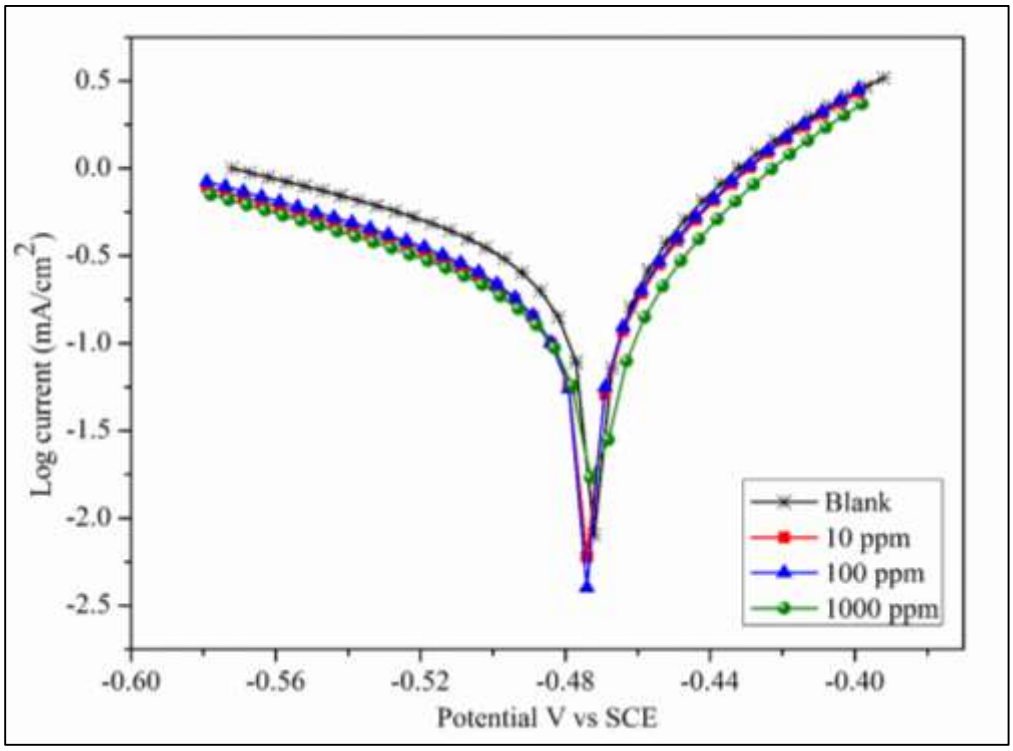

Fig. 4.27 Polarization curves for mild steel 0.5 M H_2SO_4 for selected concentrations of MPOHX

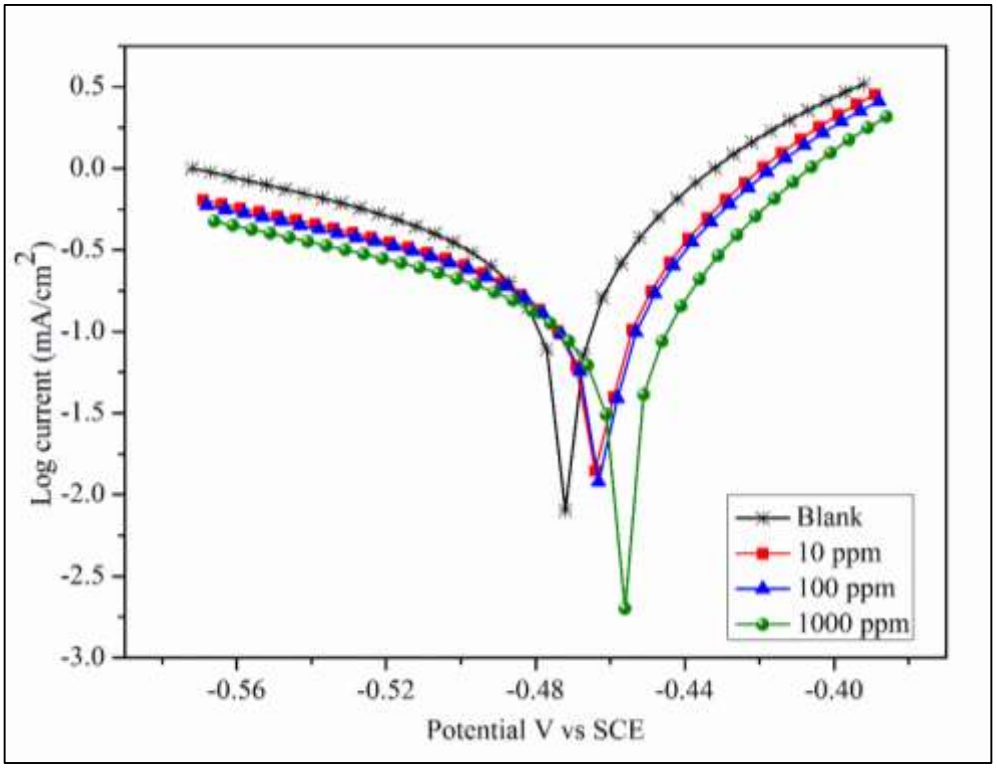

Fig. 4.28 Polarization curves for mild steel 0.5 M H_2SO_4 for selected concentrations of MPOHP

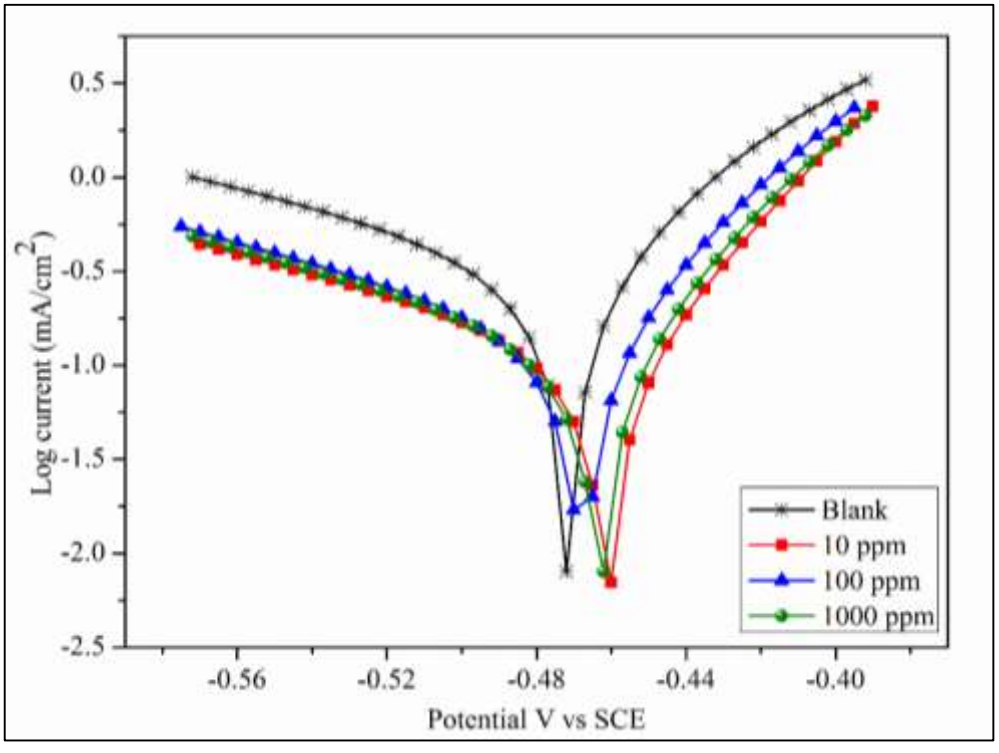

Fig. 4.29 Polarization curves for mild steel 0.5 M H_2SO_4 for selected concentrations of MPOO

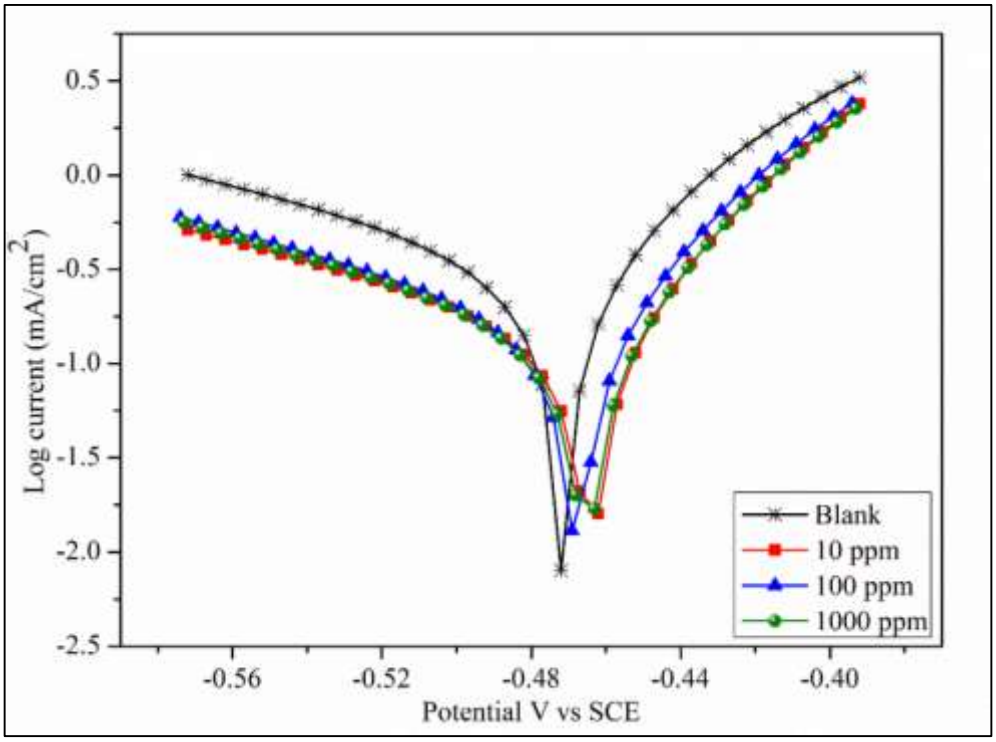

Fig. 4.30 Polarization curves for mild steel 0.5 M H_2SO_4 for selected concentrations of MPON

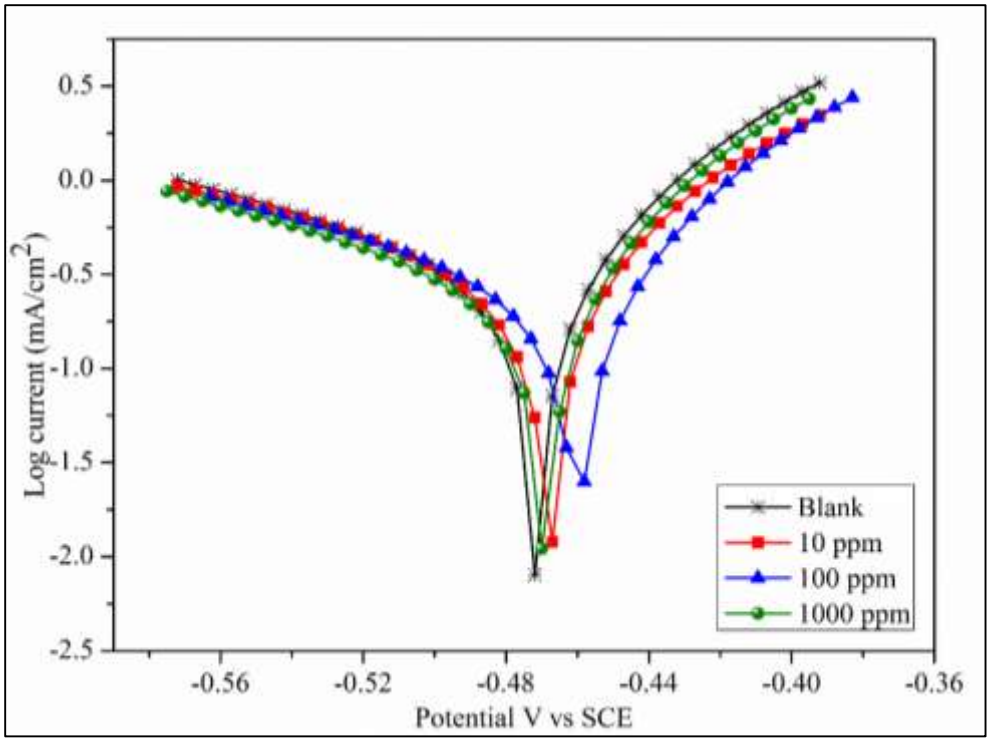

Fig. 4.31 Polarization curves for mild steel 0.5 M H_2SO_4 for selected concentrations of MPOD

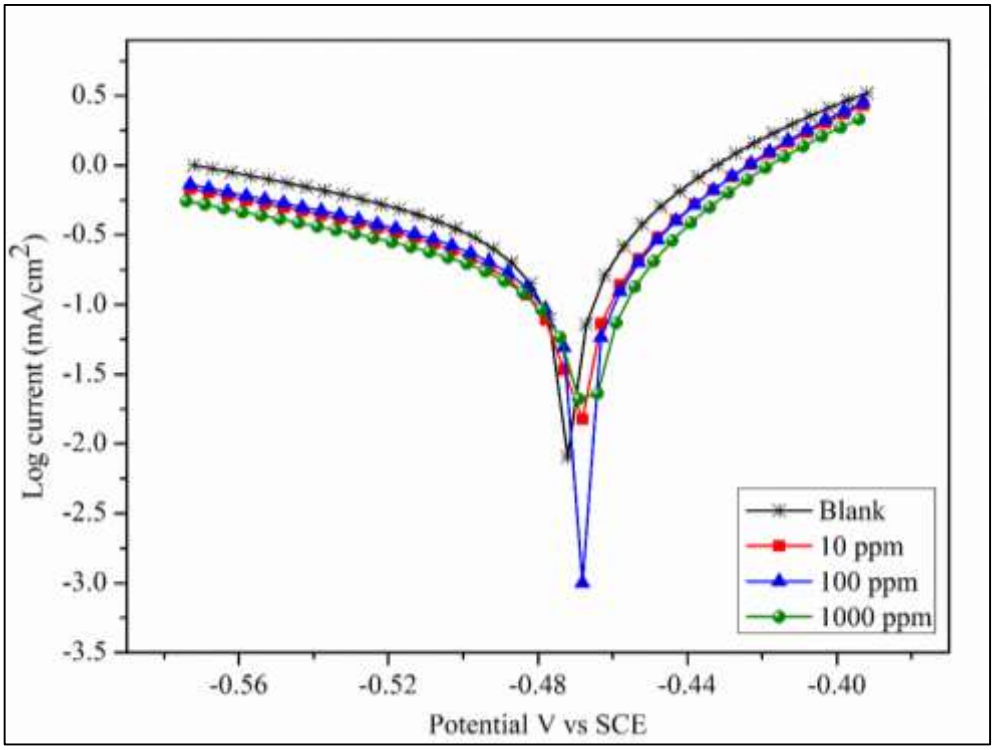

Fig. 4.32 Polarization curves for mild steel 0.5 M H_2SO_4 for selected concentrations of MPOU

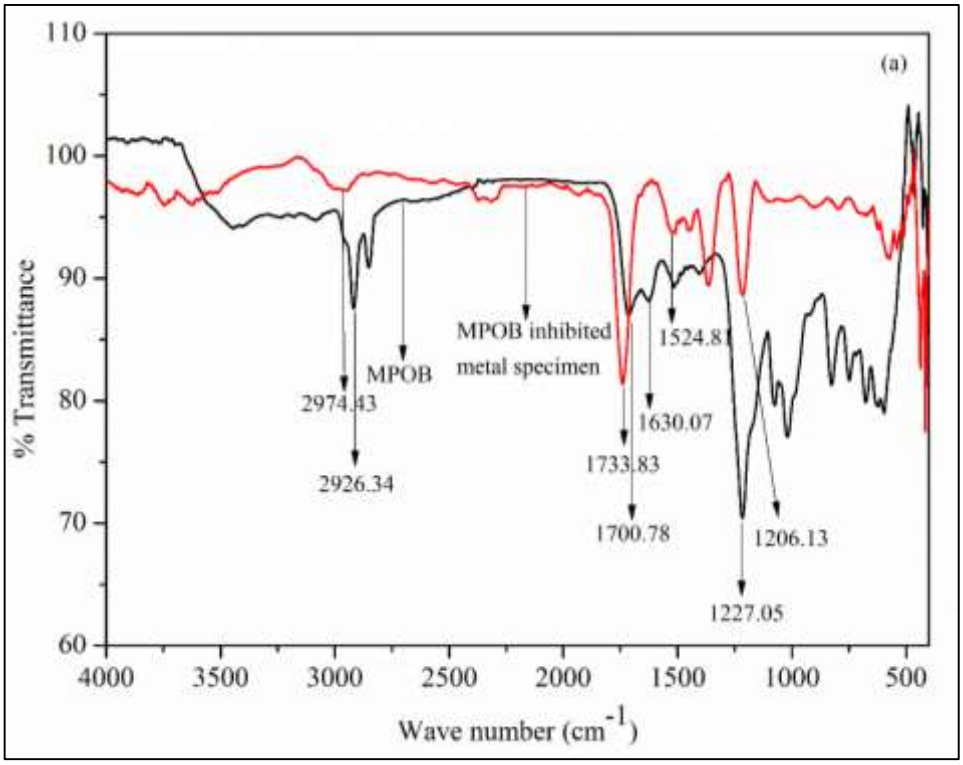

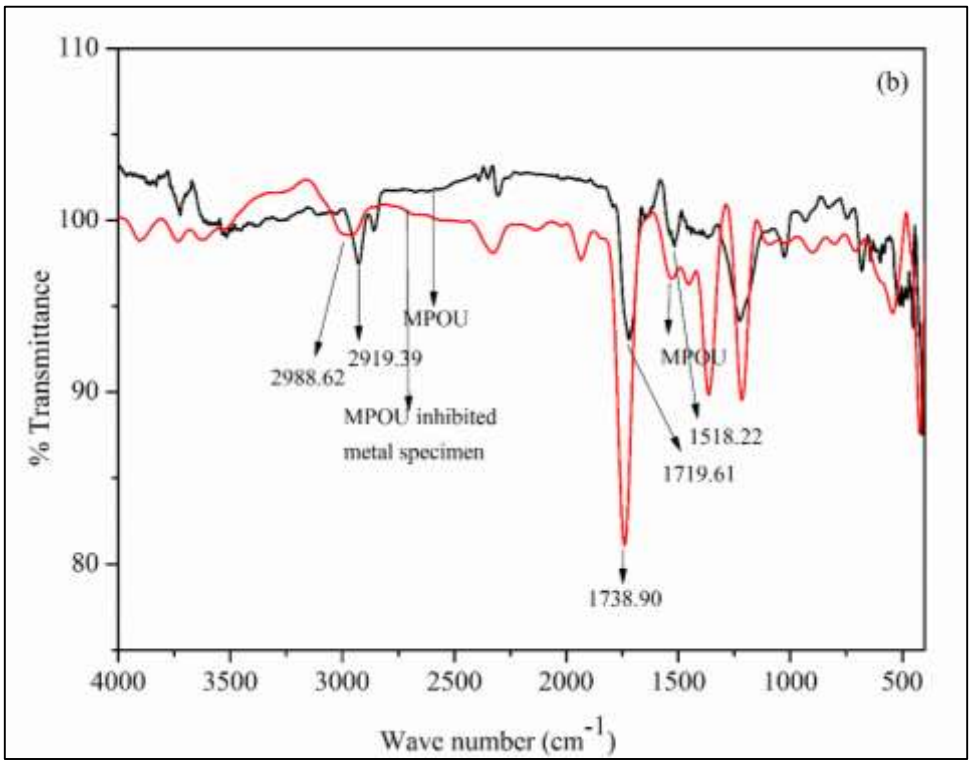

Fig. 4.33 FT-IR spectra of a) MPOB and metal inhibited b) MPOU and metal inhibited

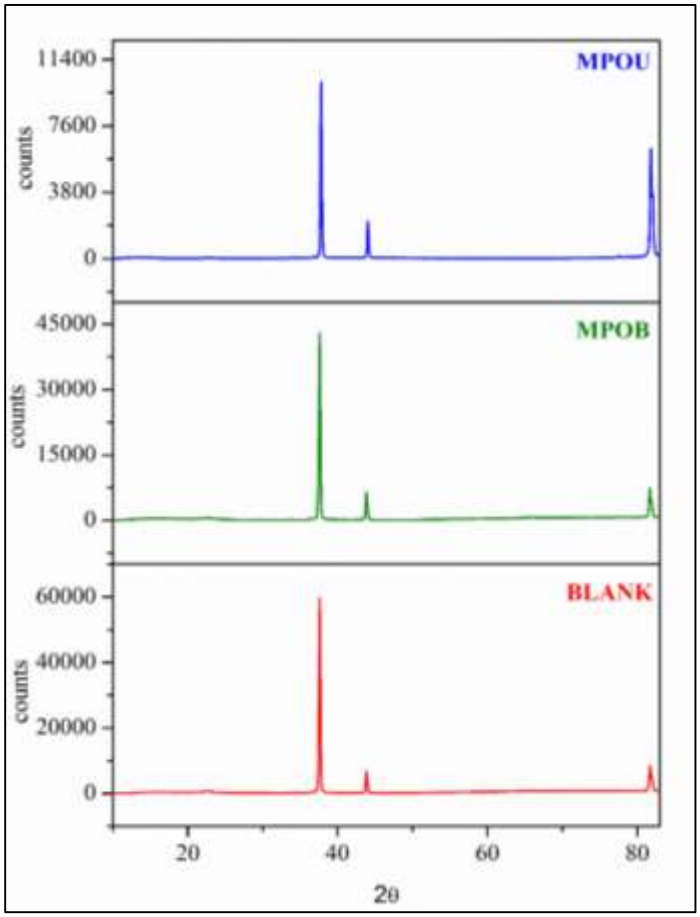

Fig. 4.34 XRD patterns of mild steel in uninhibited and inhibited medium

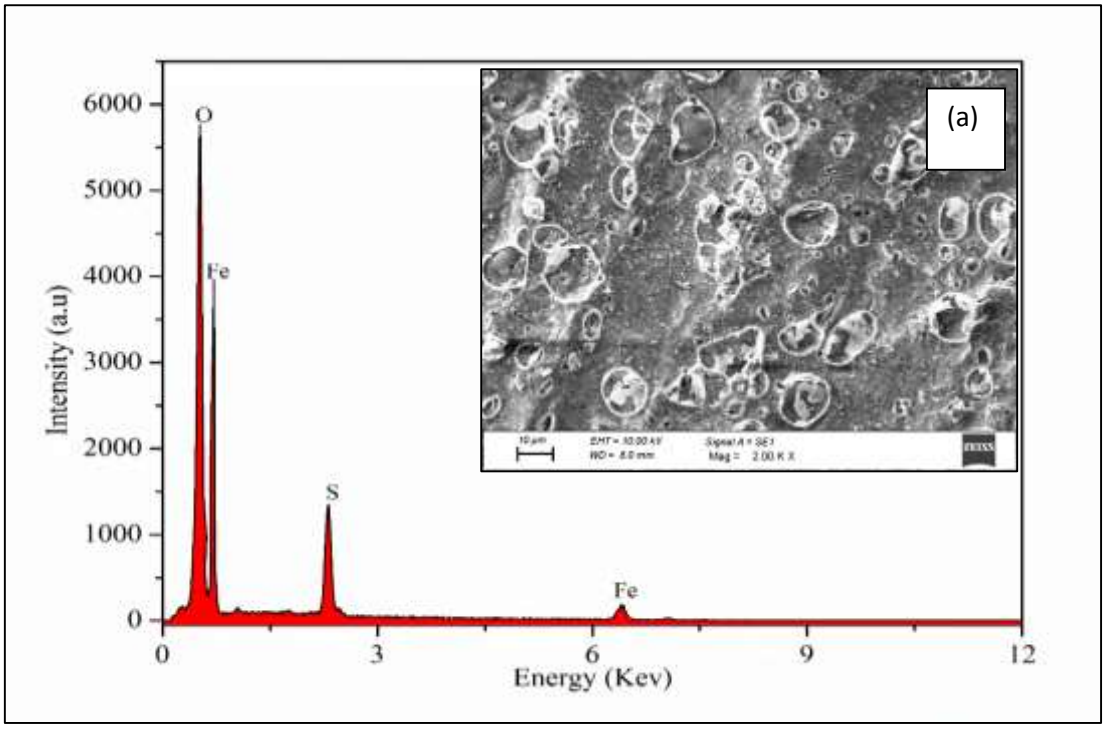

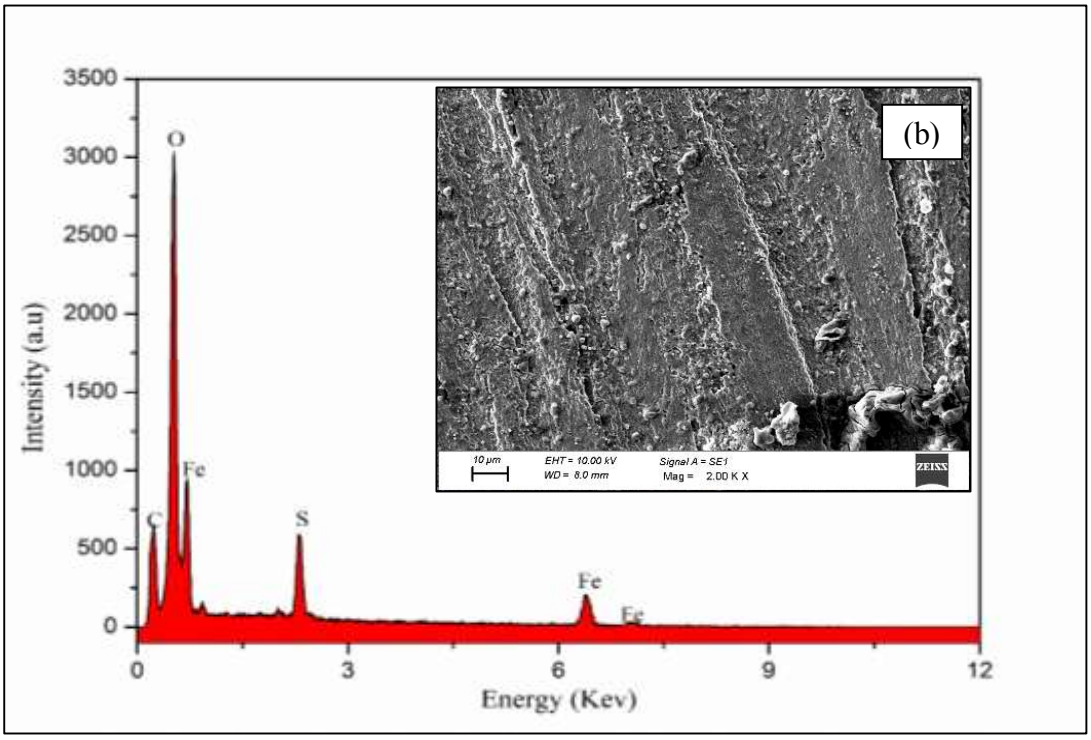

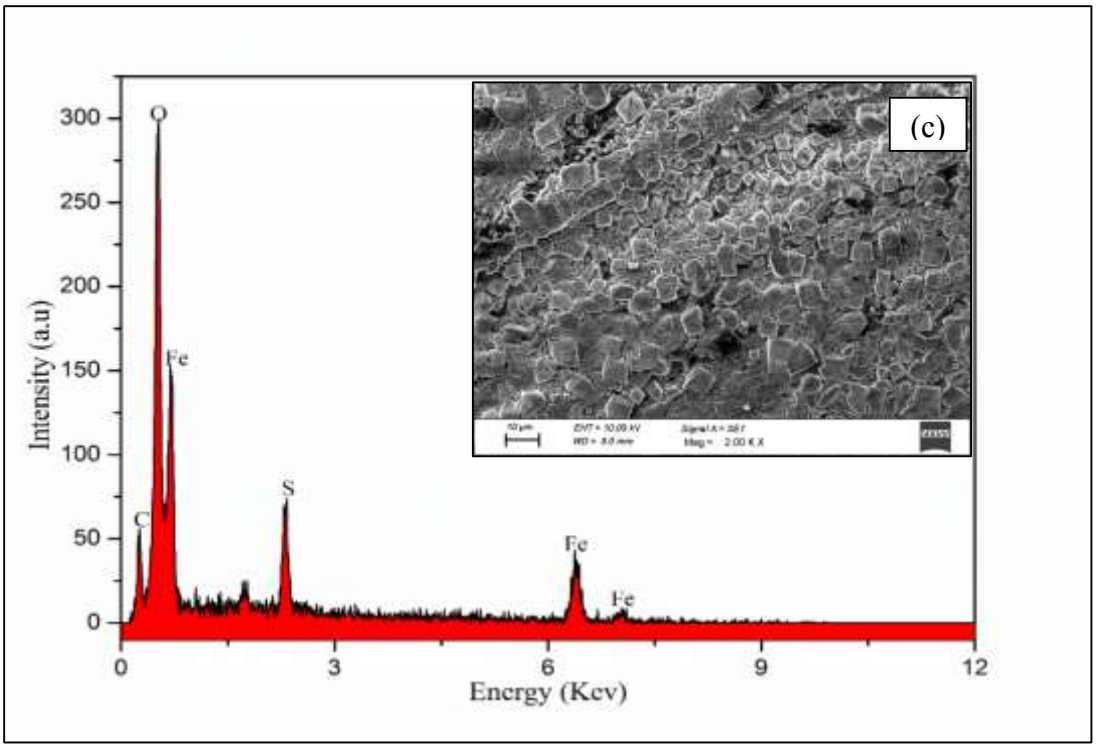

Fig. 4.35 SEM-EDS images of mild steel coupons immersed in a) 0.5 M H_2SO_4 b) MPOB inhibited medium c) MPOU inhibited medium

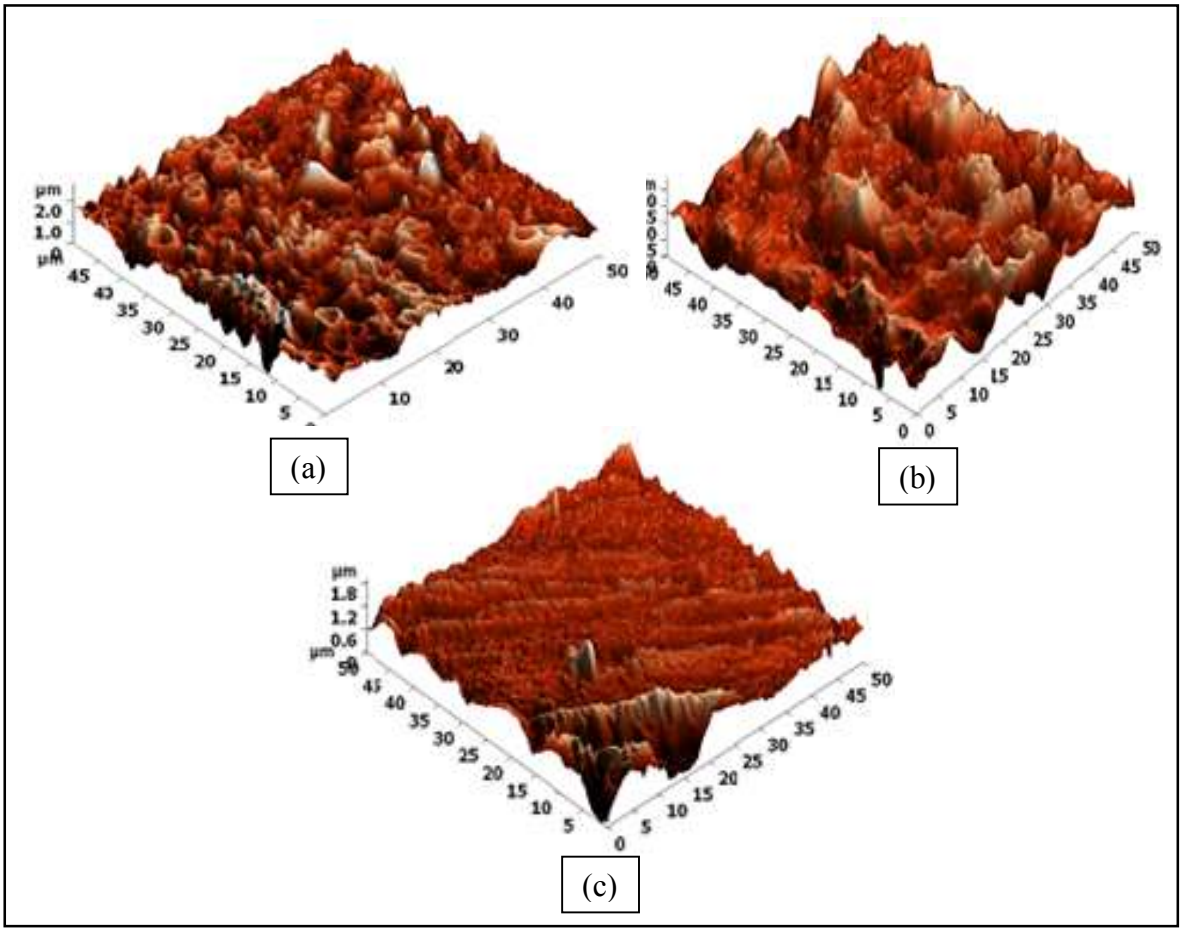

Fig. 4.36 AFM images of a) uninhibited medium b) MPOB inhibited medium c) MPOU inhibited medium

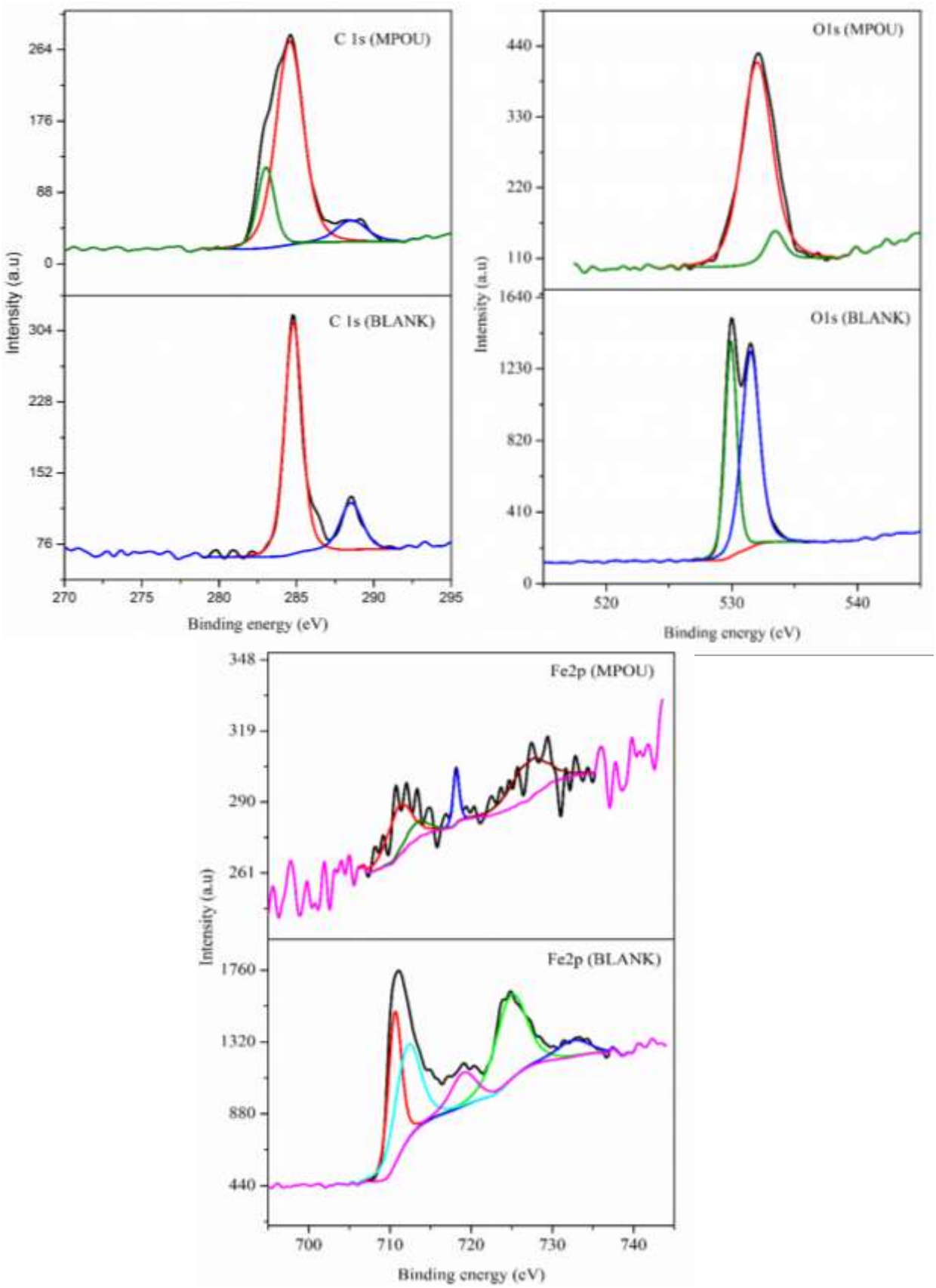

Fig. 4.37 XPS Deconvolution peak of blank and MPOU inhibited specimens

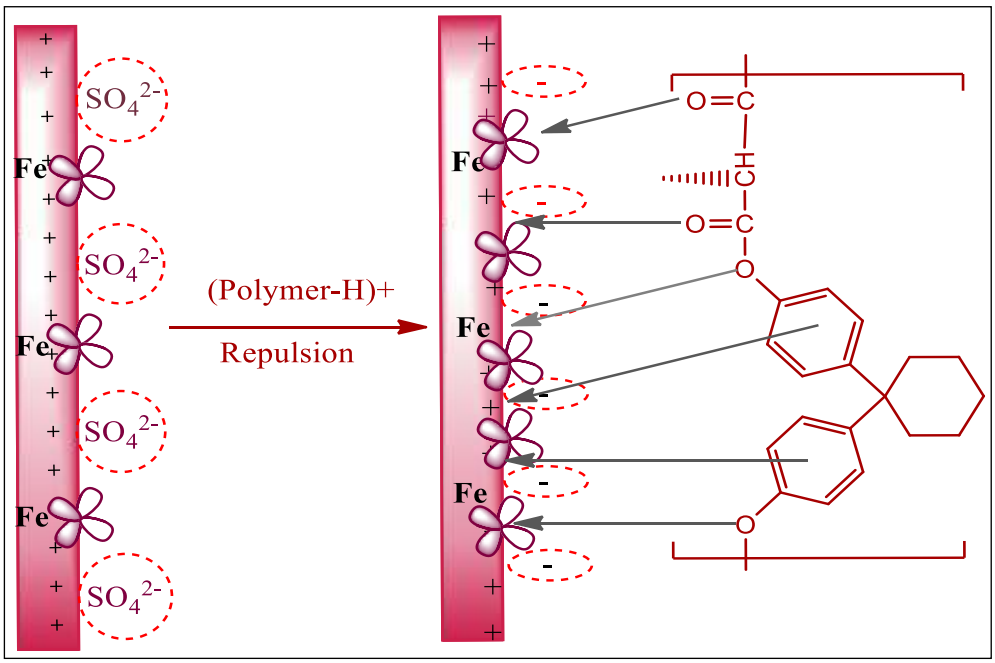

Fig. 4.38 Schematic illustration of proposed mechanism